12

Earthquake Dynamics

Raúl Madariaga
Ecole Normale Supérieure, Paris, France
Kim Bak Olsen
University of California, Santa Barbara, California, USA

1. Introduction

Earthquake source dynamics provides key elements for the prediction of strong ground motion and for understanding the physics of earthquake initiation, propagation, and healing. Early studies pioneered our understanding of friction and introduced simple models of dynamic earthquake rupture, typically using homogeneous distributions of stress and friction parameters. Classical examples of such models are the mechanical spring-and-box models proposed by Burridge and Knopoff (1967), the rectangular dislocation model proposed by Haskell (1964), and the self-similar circular rupture model introduced by Kostrov (1966). Extensive research then followed to advance our understanding of seismic rupture propagation and stress relaxation. It became clear that the correct mathematical formulation of the problem of propagation and radiation by a seismic rupture was that of a propagating shear crack as proposed by Kostrov (1964, 1966). Very soon it became clear that friction also played a fundamental role in the initiation, the development of rupture, and the healing of faults. The classical Coulombian model of a sudden drop in friction from a static to a dynamic coefficient led to an impasse, with infinite stress singularities and many other physical problems. The reason is that this model lacks an essential length scale needed to define a finite energy release rate near the rupture front.

Better models of friction at low slip rates were studied in the laboratory by Dieterich (1978, 1979) and Ruina (1983), who proposed the model of rate- and state-dependent friction. Slip weakening friction laws were introduced in dynamic rupture modeling by Ida (1972) and Andrews (1976a,b) for plane (2D) ruptures and by Day (1982b) for 3D fault models. These authors showed that slip weakening regularizes the numerical model of the rupture front, distributing stress and slip concentrations over a distance controlled by the length scale in the friction law. Ohnaka and Kuwahara (1990), Ohnaka (1996), and Ohnaka and Shen (1999) concluded that their experiments could be explained with a simple slip weakening friction law. In fact, for many practical purposes, the rate-and-state and slip weakening friction laws can be reconciled by rating that both models contain a finite length scale that controls the behavior of the rupture front (see Okubo, 1989; Dieterich and Kilgore, 1996). Extensive reviews on rupture dynamics up to 1990 have been published by Kostrov and Das (1989) and Scholz (1989).

Recent studies of rupture processes for selected earthquakes have shed new light on our understanding of earthquake ruptures. These models suggest a complexity of the rupture process that the early models of rupture in a uniformly loaded medium were unable to explain. Although, in the late 1970s, Das and Aki (1977b), Mikumo and Miyatake (1978, 1979), Madariaga (1979), and Andrews (1980, 1981) pointed out the deficiencies of the classical dislocation and crack models, it was not until the late 1980s that good-quality near-field accelerometry became available for some large earthquakes. Simultaneously, new sophisticated and efficient numerical methods, such as boundary integral equations (BIE) and finite differences (FD), provided the tools to study realistic dynamic rupture propagation in a fault subject to a heterogeneous stress field and spatially varying friction.

Heaton (1990) noticed that rupture of large earthquakes was typically characterized by pulselike behavior, where only a small part of the fault would rupture at a given instant. This result has been confirmed by a number of inversions of the slip-rate field for large earthquakes, such as the 1992 Landers earthquake in California (Cohee and Beroza, 1994; Wald and Heaton, 1994; Cotton and Campillo, 1995a). Cochard and Madariaga (1996) found that, at least for a simple velocity weakening friction law, heterogeneity could arise spontaneously in a two-dimensional homogeneous fault model as found earlier by Carlson and Langer (1989) for the Burridge and Knopoff model of sliding blocks connected by springs. Other authors studied complex fault models from a theoretical point view (Harris and Day, 1993, 1997). Beroza and Mikumo

INTERNATIONAL HANDBOOK OF EARTHQUAKE AND ENGINEERING SEISMOLOGY, VOLUME 81A

(1996) found that dynamic models with heterogeneous fault parameters tend to generate short slip duration.

In a direct modeling approach, Olsen *et al*. (1997) and Peyrat *et al*. (2001) showed that rupture propagation in a dynamic model of the 1992 Landers earthquake, would follow a complex path, completely controlled by the spatial variation of the initial stress field. Ide and Takeo (1997) estimated the constitutive friction law parameters for the 1995 Kobe earthquake from their kinematic inversion results. Computations of dynamic stress changes for the 1992 Landers, 1994 Northridge, and 1995 Kobe earthquakes (Bouchon, 1997; Day *et al*., 1998) showed highly variable distributions of stress drops. Spudich *et al*. (1998) detected coseismic changes in the slip direction for the 1995 Kobe earthquake. Nielsen *et al*. (2000) indicated that such complexity inherently arises as a result of many recurrent earthquakes on a single fault over along time span.

In this chapter we review what we believe are the important results obtained to date in the field of earthquake rupture. In Section 2 we review the early models of earthquake rupture and discuss the elastic shear fault model and fundamental friction laws. We also briefly describe the BIE and FD numerical methods for numerical modeling of dynamic rupture. In Section 3 we illustrate the most important phenomenology of simple rupture models with a single length scale for circular and rectangular fault models, including anisotropy and scaling of growth, generation of sub-shear and super-shear rupture speeds, and the numerical resolution of these models. Scaling laws for earthquake rupture are described in Section 4, including the complementary roles of friction, strength, and geometry. Section 5 shows the results of modeling the 1992 M 7.3 Landers event, including computation of a heterogeneous initial stress field and estimation of the frictional parameters. We compare the dynamic modeling results to those from kinematic models and strong motion data. Finally we discuss the importance of heterogeneity in the rupture process, including the necessity of multiple length scales, generation of self-healing pulses, and the origin of rupture complexity, and discuss the possibility of estimating friction from observations.

2. Fault Models and Friction

In this section we review some of the simpler models that have been used to model seismic ruptures: the Burridge–Knopoff (BK) model; one of its modern versions, the cellular automata (CA) model; and what is still the most useful kinematic description of an earthquake—the dislocation model. Then we introduce the theory behind the elastic shear fault model and basic friction laws. Finally, we briefly describe the concepts of the two numerical methods that have dominated the field of modeling of dynamic rupture: the boundary integral element (BIE) and finite-difference (FD) methods.

2.1 Classical Dynamic Model Assumptions: Burridge–Knopoff and its Successors

Burridge and Knopoff (1967) pioneered dynamic rupture behavior by studying a mechanical model composed of a chain of N blocks coupled by horizontal springs of stiffness κ sliding on a frictional surface that delays the motion of the blocks. The one-dimensional array of springs is connected by individual leaf springs of stiffness k to a rigid driving bar that moves horizontally with a constant velocity. For all reasonable friction laws in which friction decreases once slip starts, the blocks in the BK models move by stick–slip with long periods of stress accumulation and sudden jerky displacement. This model is an analogue or "toy" model of an earthquake fault that is loaded by slow plate motion and locked by friction except in brief intervals when the loading stress overcomes friction at the interface. When this model is loaded at sufficiently high stresses, rupture starts by slip on one of the blocks of the chain and spreads rapidly to neighboring blocks. Until the 1980s this model was a simple and curious analogue to an earthquake rupture, and most seismologists believed that slip episodes would always spread to all the blocks of the system. However, Cao and Aki (1984) and Carlson and Langer (1989) found numerically that this was not the case. Instead, they discovered that very complex rupture histories would develop in this model starting from a nominally homogeneous system. Actually, the BK model has two types of ruptures: local events that tend to smooth the system; and long events that propagate along the whole chain and wrap around it when cyclic boundary conditions are used. These large, soliton-like events roughen the system, as shown by Schmittbuhl *et al*. (1996). Small events in this system obey a Gutenberg–Richter type power law for the number of events with respect to the number of sliding blocks that participate in any individual event. Large, macroscopic events have a completely different distribution centered around the total number of events in the chain. This model has become a paradigm for the dynamic origin of complexity on a fault, although several authors pointed out a number of reasons why this was not a very realistic model of earthquakes. The most serious problem is that it does not radiate and dissipate seismic energy. Rice and Ben Zion (1996) suggested that small event complexity in this system was probably due to the lack of continuum limit of this model.

An interesting class of models inspired from the BK model, but much simpler to compute, consists of the cellular automata models (see, e.g., Wolfram, 1986). Using different versions of cellular automata, it is possible to reproduce the power law distribution of earthquake statistics (Gutenberg and Richter law). More interestingly, certain interacting dynamical systems may spontaneously evolve into a critical state, producing earthquakes of all sizes. This is the so-called self-organized critical state (see, e.g., Bak *et al*., 1987). A major problem with cellular automata models is that they lack scales for time and/or length. Time evolution occurs by discrete quasi-static steps so that—at least in the version known to us—they do not include dynamic

effects. As will become apparent in a later section, length and time scales are essential for physically correct modeling of the forces underlying the dynamic behavior. Although these models are for the moment too simple for simulating the observed radiation from a real earthquake, there is no doubt that these concepts will play a major role in future earthquake studies.

In order to understand the physics of the dynamic behavior, we turn to the theory of an elastic shear fault, starting from the simplest approximation.

2.2 The Dislocation Model

In spite of much recent progress in understanding the dynamics of earthquake ruptures, the most widely used models for interpreting seismic radiation are the so-called dislocation models. In these models the earthquake is simulated as the kinematic spreading of a displacement discontinuity (slip or dislocation in seismological usage) along a fault plane. In its most general version, slip in a dislocation model is completely arbitrary and rupture propagation may be as general as desired. In this version the dislocation model is a perfectly legitimate description of an earthquake as the propagation of a slip episode on a fault plane. It must be remarked, however, that not all slip distributions are physically acceptable: as shown by Madariaga (1978), most dislocation models present unacceptable features such as interpenetration of matter, release unbounded amounts of energy, and so on. For these reasons, dislocation models must be considered as a useful intermediate step in the formulation of a physically acceptable dynamic fault model.

Dislocation models are very useful in the inversion of near-field accelerograms (see, e.g., Cohee and Beroza, 1994; Wald and Heaton, 1994; Cotton and Campillo, 1995a; Mikumo and Miyatake, 1995; and many others). Radiation from a dislocation model can be written as a functional of the distribution of slip on the fault. In a simplified form a seismogram $u(x,t)$ at an arbitrary position x can be written as

$$u(r,t) = \int_0^t \int_{S_\xi} \Delta u(\xi,\tau) G(x-\xi, t-\tau)\, d\xi\, d\tau \qquad (1)$$

where $\Delta u(\xi,\tau)$, the slip on the fault, is a function of space and time, and $G(x,t)$ is the Green tensor that may be computed using simple layered models of the crustal structure, or more complex numerical (for example, FD) simulations. Functional (1) is linear in slip amplitude but very nonlinear with respect to rupture propagation, which is implicit in the time dependence of δu. For this reason, in most inversions the kinematics of the rupture process (position of rupture front as a function of time) is assumed to propagate at constant rupture velocity from the hypocenter. Different approaches have been proposed in the literature in order to invert approximately for variations in rupture speed about the assumed constant rupture velocity (see, e.g., Wald and Heaton, 1984; Cotton and Campillo, 1995a). The slip history on the fault can then be used to compute the history of stress on the fault by a procedure originally proposed by Mikumo and Miyatake (1979). This method has been used extensively in recent years to estimate the state of stress on a fault (see, e.g., Bouchon, 1997; Ide and Takeo, 1997; Olsen *et al*., 1997; Day *et al*., 1998; Guatteri and Spudich, 1998a,b; among many others).

The most important dislocation model was introduced by Haskell (1964). In this model, shown in Figure 1, a uniform displacement discontinuity spreads at constant rupture velocity inside a rectangular-shaped fault. At low frequencies, or wavelengths much longer than the size of the fault, this model is a reasonable approximation to a seismic rupture. In Haskell's model, at time $t=0$ a line of dislocation of width W appears suddenly and propagates along the fault length at a constant rupture velocity until a region of length L of the fault has been broken. As the dislocation moves, it leaves behind a zone of constant slip D. The fault area $L \times W$ times the slip D and the rigidity μ of the medium defines the seismic moment $M_0 = \mu DLW$ of this model. Haskell's model captures some of the most important features of an earthquake and has been used extensively to invert for seismic source parameters from near-field and far-field seismic and geodetic data. The complete seismic radiation for Haskell's model was computed by Madariaga (1978) who showed that, because of the stress singularities around the edges, the Haskell model fails at high frequencies, as was noted by Haskell (1964) himself. All dislocation models with constant slip will have the same problems at high frequencies, although they can be improved by tapering the slip discontinuity near the edges of the fault, as proposed by Sato and Hirasawa (1973). Even better dislocation models can be obtained by taking into account the kinematics of rupture front propagation as proposed by Spudich and Hartzell (1984) and Bernard and Madariaga (1984). Kinematic models have played a mayor role in the quantification of earthquakes and in the inversion of seismic data, a subject that we cannot develop in depth in this chapter.

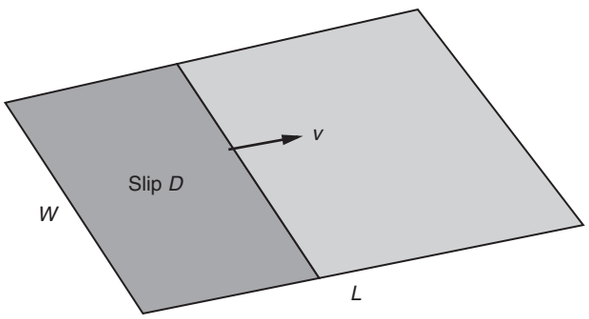

FIGURE 1 The Haskell kinematic earthquake model, probably the simplest possible earthquake model. The fault has a rectangular shape and a linear rupture front propagates from one end of the fault to the other at constant rupture speed v. Slip in the broken part of the fault is uniform and equal to D.

2.3 Elastic Shear Fault Model

Let us now study the main features of a properly posed source model in a simple homogeneous elastic model of the Earth. Expansion to more complex elastic media, including realistic wave propagation media, poses no major technical difficulties except, of course, that computation time may become very long.

Consider the 3D elastic wave equation:

$$\rho \frac{\partial^2}{\partial t^2}\mathbf{u} = \boldsymbol{\nabla}\cdot\sigma, \tag{2}$$

where $\mathbf{u}(\mathbf{x}, t)$ is the displacement vector field, a function of both position $\mathbf{x}$ and time t, and $\rho(\mathbf{x})$ is the density of the elastic medium. Associated with the displacement field $\mathbf{u}$ the stress tensor $\sigma(\mathbf{x}, t)$ is defined by

$$\sigma = \lambda\boldsymbol{\nabla}\cdot\mathbf{u}\,\mathbf{I} + \mu\left[(\boldsymbol{\nabla}\mathbf{u}) + (\boldsymbol{\nabla}\mathbf{u})^{\mathrm{T}}\right] \tag{3}$$

where $\lambda(\mathbf{x})$ and $\mu(\mathbf{x})$ are Lamé elastic constants, $\mathbf{I}$ is the identity matrix, and superscript T indicates matrix transpose. We can transform this system into a more symmetric velocity–stress formulation (Madariaga, 1976; Virieux and Madariaga, 1982; Virieux, 1986):

$$\begin{aligned}\rho\frac{\partial}{\partial t}\mathbf{v} &= \boldsymbol{\nabla}\cdot\sigma + \mathbf{f}\\ \frac{\partial}{\partial t}\sigma &= \lambda\boldsymbol{\nabla}\cdot\mathbf{v}\,\mathbf{I} + \mu\left[(\boldsymbol{\nabla}\mathbf{v}) + (\boldsymbol{\nabla}\mathbf{v})^{\mathrm{T}}\right] + \dot{\mathbf{m}}\end{aligned} \tag{4}$$

where $\mathbf{v}(\mathbf{x}, t)$ is the particle velocity vector; and $\mathbf{f}(\mathbf{x})$ and $\mathbf{m}(\mathbf{x})$ are the force and moment source distributions, respectively.

2.3.1 Boundary Conditions on the Fault

Assume that the earthquake occurs on a fault surface of normal n in the previous elastic medium. Due to frictional instability, a rupture zone can spread along the fault; let $\Gamma(t)$ be this rupture zone at time t. In general, $\Gamma(t)$ is a collection of one or more rupture zones propagating along the fault.

The main feature of a seismic rupture is that, at any point $\mathbf{x}$ inside the rupture zone $\Gamma(t)$, displacement and particle velocities are discontinuous. Let

$$\mathbf{D}(\mathbf{x}, t) = \mathbf{u}^{+}(\mathbf{x}^{+}, t) - \mathbf{u}^{-}(\mathbf{x}^{-}, t) \tag{5}$$

be the slip vector across the fault, i.e., the jump in displacement between the positive and the negative side of the fault. The notation $\mathbf{x}^{\pm}$ indicates a point immediately above or below the fault, and $\mathbf{u}^{\pm}$ are the corresponding displacements.

Slip D is associated with a *change in the traction* $\mathbf{T} = \sigma\cdot\mathbf{e}_z = [\sigma_{zx}, \sigma_{yz}, \sigma_{zz}]$ across the fault through the solution of the wave equation (4):

$$\Delta\mathbf{T}(\mathbf{x}, t) = \Delta\boldsymbol{\Sigma}[\mathbf{D}] \qquad \text{for} \qquad \mathbf{x}\in\Gamma(t) \tag{6}$$

where $\Delta\boldsymbol{\Sigma}[\mathbf{D}]$ is a shorthand notation for a functional of $\mathbf{D}$ and its temporal and spatial derivatives.

2.4 Friction

The main assumption in seismic source dynamics is that traction across the fault is related to slip at the same point through a *friction law* that can be expressed in the general form

$$\mathbf{T}(\mathbf{D}, \dot{\mathbf{D}}, \theta_i) = \mathbf{T}_{\text{total}} \qquad \text{for} \qquad \mathbf{x}\in\Gamma(t) \tag{7}$$

such that friction $\mathbf{T}$ is a function of at least slip, but an increasing amount of experimental evidence shows that it is also a function of slip rate $\dot{\mathbf{D}}$ and several state variables denoted by θ_i, $i = 1, \ldots, N$. The traction that appears in friction laws is the total traction $\mathbf{T}_{\text{total}}$ on the fault, which can be expressed as the sum of preexisting stress $\mathbf{T}^0(\mathbf{x})$ and the stress change $\Delta\mathbf{T}$ due to slip on the fault obtained from Eq. (6). The prestress is caused by tectonic load of the fault and will usually be a combination of purely tectonic loads due to internal plate deformation, plate motion, etc., and the residual stress field remaining from previous seismic events on the fault and its vicinity.

Using Eq. (6), we can now explicitly formulate the friction law on the fault [Eq. (7)]:

$$\mathbf{T}(\mathbf{D}, \dot{\mathbf{D}}, \theta_i) = \mathbf{T}^0(\mathbf{x}) + \Delta\mathbf{T}(\mathbf{x}, t) \qquad \text{for} \qquad \mathbf{x}\in\Gamma(t) \tag{8}$$

Friction as defined by Eq. (8) is clearly a vector. For the appropriate study of a shear fault we need to write Eq. (8) as a system of two equations. Archuleta and Day (1980), Day (1982a,b), and Spudich (1992) used a very simple approach that will certainly have to be refined in the future, assuming that slip rate and traction are antiparallel, i.e.,

$$\mathbf{T}(\mathbf{D}, \dot{\mathbf{D}}, \theta_i) = -T(D, \dot{D}, \theta_i)\mathbf{e}_V \tag{9}$$

where $\mathbf{e}_V = \dot{\mathbf{D}}/\|\dot{\mathbf{D}}\|$ is a unit vector in the direction of instantaneous slip rate. With this assumption, the boundary condition reduces Eq. (8) to the special form

$$-T(D, \dot{D}, \theta_i)\mathbf{e}_V = \mathbf{T}^0(\mathbf{x}) + \Delta\mathbf{T}(\mathbf{x}, t) \quad \text{for} \quad \mathbf{x}\in\Gamma(t) \tag{10}$$

Figure 2a shows the vector diagram implied by this equation. The only fixed vector in this diagram is the prestress, which is assumed to be known. Friction and slip rate are collinear but antiparallel. Stress change $\Delta\mathbf{T}$ is in general collinear neither with prestress nor with friction. Recently, Spudich (1992), Cotton and Campillo (1995b), and Guatteri and Spudich (1998b) analyzed expression (10) and studied several recent earthquakes, showing that slip directions were not always parallel to stress drop. These rake rotations may also have information about the absolute stress levels (Spudich, 1992; Guatteri and Spudich, 1998b).

In most rupture models the above "vector" friction is simplified to a "scalar boundary condition," in which slip is only allowed in the direction of the initial stress, which is everywhere parallel to the x axis, i.e., $\mathbf{T}^0(\mathbf{x}) = [T_x^0(\mathbf{x}), 0]$ and $\mathbf{D}(\mathbf{x}, t) = [D_x(\mathbf{x}, t), 0]$; then the scalar components are simply related by

$$\Delta T_x(\mathbf{x}, t) = T(D, \dot{D}, \theta_i) - T_x^0(\mathbf{x}) \qquad \text{for} \qquad \mathbf{x}\in\Gamma(t) \tag{11}$$

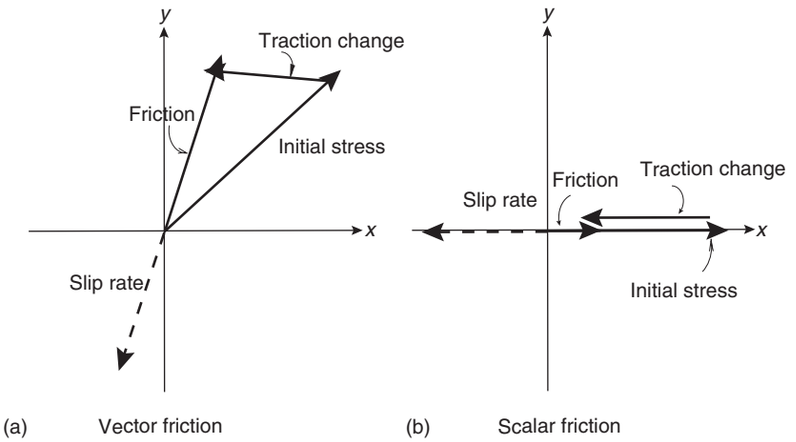

FIGURE 2 Diagram showing the relation between initial stress, slip rate, friction, and traction change for the vector (a) and scalar (b) approximations to friction on the fault plane. In the scalar case, traction change corresponds to the usual definition of stress drop. (Reproduced with permission from Madariaga *et al*., 1998; fig. 1, p. 1185.)

This boundary condition, which may be graphically described as if the fault had "rails" aligned in the x direction, has been applied in most 3D source models, starting with Madariaga (1976).

2.5 Friction Laws

Both boundary conditions (10) and (11) require a friction law that relates scalar traction T to slip, its derivatives, and possible state variables. For more details, see Dieterich (1978, 1979) and Rice and Ruina (1983), but see also Ohnaka (1996) for an alternative point of view.

Let us first discuss the simple slip weakening friction law introduced by Ida (1972). It is an adaptation to shear faulting of the Barenblatt–Dugdale friction laws used in hydrofracturing and tensional (mode I) cracks. In this friction law, slip is zero until the total stress reaches a peak value (yield stress) that we denote by T_u. Once this stress has been reached, slip D starts to increase from zero and $T(D)$ decreases linearly to zero as slip increases:

$$\begin{aligned} T(D) &= T_u\left(1-\frac{D}{D_c}\right)+T_f \qquad \text{for} \qquad D<D_c \\ T(D) &= T_f \qquad\qquad\qquad\qquad\quad \text{for} \qquad D>D_c \end{aligned} \tag{12}$$

where D_c is a characteristic slip distance and T_f is the residual friction at high slip rate, sometimes called the "kinematic" friction. There is a lot of discussion in the literature about how large this residual friction is. Many authors, following the observation that there is a very broad heat flow anomaly across the San Andreas fault in California, have proposed that faults are "weak," meaning that T_f is close to zero. Other authors propose that kinematic friction is high and faults are strong. We cannot go into any detail about this discussion here: interested readers may consult the papers by Scholz (2000) and Townend and Zoback (2000). For most applications of earthquake dynamics, only stress change is important, so that without loss of generality we can assume that $T_f = 0$ in much of the following. Let us remark, however, that Spudich (1992), Guatteri and Spudich (1998a), and Spudich *et al*. (1998) have found some evidence for absolute stress levels from nonparallel stress drop and slip of the 1995 Kobe earthquake in Japan.

The slip weakening friction law (12) has been used in numerical simulations of rupture by Andrews (1976a,b), Day (1982b), Harris and Day (1993), Fukuyama and Madariaga (1998), Madariaga *et al*. (1998), and many others. Slip weakening at small slip is *absolutely necessary for the friction law to be realizable*, otherwise stress would become unbounded near the rupture front, violating energy conservation so that seismic ruptures could only spread at either S, Rayleigh, or P wave velocities until they stop. Of course, in numerical implementations stress is never infinite, so that rupture velocity is numerically limited. In many earlier studies of earthquake dynamics, a simpler version of Eqs. (12) was used in which D_c was effectively zero. This numerical version of slip-weakening has been called the Irwin criterion by Das and Aki (1977a) and has been widely used by many authors although it is obviously grid-dependent (see, e.g., Virieux and Madariaga, 1982).

Once slip is larger than the slip weakening distance D_c, friction becomes a function of slip rate $\dot{D}$ and one or more state variables that represent the memory of the interface to previous slip. A very simple *rate-dependent friction law* was proposed by Burridge and Knopoff (1967) and has been used extensively in simulations by Carlson and Langer (1989) and their colleagues and by Cochard and Madariaga (1986):

$$T(\dot{D}) = T_s\frac{V_0}{V_0+\dot{D}}+T_f \tag{13}$$

where V_0 is a characteristic slip velocity and $T_s < T_u$ is the limit of friction when slip rate decreases to zero. The applicability of rate weakening to seismic ruptures is much more controversial than slip weakening, although there is plenty of indirect evidence for its presence in seismic faulting. Heaton (1990) proposed that it was the cause of short rise times; rate-dependence at steady slip velocities is also an intrinsic part of the friction laws proposed by Dieterich (1978) and Ruina (1983), which will be reviewed in the following.

The slip weakening and slip rate weakening behavior described above can be combined if for any value of D and $\dot{D}$ the larger of expressions (12) and (13) is selected. Instead of writing a complex expression, it is simpler to show the friction law graphically in Figure 3 in the form of a law where friction depends on the two state variables slip and slip rate. The friction law described above allows rupture propagation that is completely controlled by the complex nonlinear interaction of

1. The initial stress field $\mathbf{T}^0$ in (8).
2. The distribution of yield frictional resistance T_u in Eqs. (12) and (13).
3. The parameters D_c, T_s, and V_0 of the friction laws in Eqs. (12) and (13).

As mentioned earlier, most recent work on friction has been concentrated in a class of friction laws that depend both on slip rate and state variables. These laws were developed from laboratory experiments at low slip rates by Dieterich (1978, 1979) and Ruina (1983).

Typically, a rate-and-state dependent friction law can be expressed by

$$T(\dot{D}, \theta) = \theta + \tau(\dot{D}) \tag{14}$$

where $\tau(\dot{D})$ is the instantaneous response of friction to slip rate changes ("the direct effect"). The state variable θ represents the weakening of the interface with time and in general it is considered to satisfy an evolution equation of the form

$$\dot{\theta} = \frac{V_0}{L} G(\dot{D}, \theta) \tag{15}$$

Here L is a *weakening distance* that measures how much slip will occur before the friction weakens to the steady state value; V_0 is reference slip rate. There are many versions of these friction laws, but the main features are not very different from slip weakening, at least at the high slip rates that occur near the rupture front. Computations by Dieterich and Kilgore (1996) show that the slip weakening distance for rate-and-state dependent friction is roughly $D_c \simeq 4L$, an approximation also found by Gu and Wong (1991). Although rate-and-state dependent friction is very important for the study of rupture initiation and repeated ruptures on a fault surface, its features are indistinguishable from simpler slip-dependent and rate-dependent friction laws during the dynamic part of seismic ruptures.

2.6 The Boundary Integral Element Method

An essential requirement in studying dynamic faulting is an accurate and robust method for the numerical modeling of wave

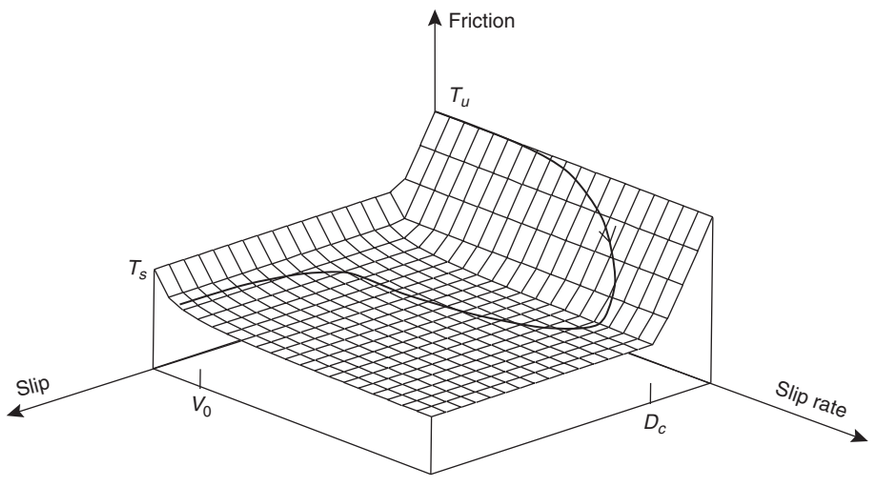

FIGURE 3 Slip- and slip rate-dependent friction law. For values of stress less than the peak static friction (T_u), slip and slip rate are zero. Once slip begins, stress is a function of both slip and slip rate described by the friction surface $T(D, \dot{D})$. Slip weakening is measured by D_c, rate weakening by V_0. The continuous curve shows the typical stress trajectory of a point on the fault. (Reproduced with permission from Madariaga *et al*., 1998; fig. 2, p. 1185.)

propagation that can also accurately handle the nonlinear boundary conditions on the fault surface. One of the important methods is the boundary integral equation (BIE) method. The BIE method was pioneered in 2D by Das and Aki (1977a,b) in the so-called direct version. It was later extended to 3D by Das (1980, 1981) and improved by Andrews (1985). A new version of the BIE method, the so-called indirect, or displacement discontinuity, method, was proposed by Koller *et al.* (1992). The indirect method was improved by the removal of strong singularities by a number of authors (e.g., Fukuyama and Madariaga, 1995, 1998; Geubelle and Rice, 1995; Cochard and Madariaga, 1996; Bouchon and Streiff, 1997). Following Fukuyama and Madariaga (1998), the integral equations for a shear fault can be expressed as

$$
\begin{aligned}
&T_\alpha(x_1, x_2, t) \\
&\quad = \frac{3\mu}{\pi} \int\int_{S^+} \frac{r_{,\alpha}}{r^2} \int_1^\kappa \tau D_{\beta,\beta}(\xi_1, \xi_2, \|t - vr/c_T\|)\, d\tau\, d\xi_1\, d\xi_2 \\
&\qquad + \frac{5\mu}{4\pi} \int\int_{S^+} \frac{r_{,\alpha}}{r^2} D_{\beta,\beta}(\xi_1, \xi_2, \|t - r/c_T\|)\, d\xi_1\, d\xi_2 \\
&\qquad - \frac{\kappa^2\mu}{\pi} \int\int_{S^+} \frac{r_{,\alpha}}{r^2} D_{\beta,\beta}(\xi_1, \xi_2, \|t - r/c_L\|)\, d\xi_1\, d\xi_2 \\
&\qquad - \frac{\mu}{4\pi} \int\int_{S^+} \frac{r_{,\beta}}{r^2} D_{\alpha,\beta}(\xi_1, \xi_2, \|t - r/c_T\|)\, d\xi_1\, d\xi_2 \\
&\qquad + \frac{\mu}{4c_T\pi} \int\int_{S^+} \frac{r_{,\alpha}}{r} \dot{D}_{\beta,\beta}(\xi_1, \xi_2, \|t - r/c_T\|)\, d\xi_1\, d\xi_2 \\
&\qquad - \frac{\mu}{2c_T} \dot{D}_\alpha(x_1, x_2, t) \qquad (16)
\end{aligned}
$$

where μ is rigidity, c_L and c_T are *P*- and *S*-wave velocities, respectively, $\kappa = c_T/c_L$, ρ is density, $r = |\mathbf{x} - \mathbf{xi}|$, $r_{,i} = (x_i - \xi_i)/r$, and $\| a \|$ is a shorthand notation meaning that the slip functions D are evaluated only for positive values of a. S^+ represents the upper surface of the crack. The Greek indices α and β can be either 1 or 2. Each term in this system of boundary integral equations has a simple interpretation. The first four terms are near-field effects due to the horizontal gradient of slip. The fifth term represents "far-field" or high-frequency *S*-wave radiation. The last term is the radiation damping due to the emission of *S*-waves in the direction normal to the fault. In order to solve the integral equation (16) numerically for shear faults, a discretization using interpolation functions has to be introduced. Traditionally in BIE high-order spatial interpolation and very low-order interpolation in time are adopted (see, e.g., Hirose and Achenbach, 1989; Koller *et al.*, 1992). This was the method adopted for antiplane cracks by Cochard and Madariaga (1996) or by Fukuyama and Madariaga (1995, 1998) for 3D faulting. Since high-order spatial interpolations lead to implicit equations in time that are almost impossible to solve in the presence of nonlinear friction on the fault, several implementations use simpler piecewise constant interpolation of slip velocity. This leads to a formulation of crack problems that Cruse (1988) calls the displacement discontinuity method. With this interpolation, the slip gradient $D_{\beta,\alpha}$ is sharply localized at the boundaries of the grid elements.

BIE methods are excellent for the study of earthquake initiation and the transition from accelerated fault creep to fully dynamic rupture propagation. A problem with the BIE method for the simulation of dynamic earthquake ruptures is the relatively large requirement for computer memory (though not of computer time) and a need for explicit computation of the operator $\Delta\boldsymbol{\Sigma}$. Also, at least in their current implementations, BIE methods cannot be used in heterogeneous media, but can be used for complex fault geometries and homogeneous half-spaces. Aochi *et al.* (2000) have recently extended the BIEM to handle complex faults with noncoplanar segments. They studied rupture propagation for the 1992 Landers earthquake and showed that rupture can jump between segments under some restrictive conditions.

2.7 The Finite Difference (FD) Method

The other numerical method widely used for numerical modeling of dynamic wave propagation is the finite difference (FD) method. The finite difference (FD) method was introduced by Madariaga (1976) and Andrews (1976a,b) for the study of seismic ruptures and was developed by numerous authors (e.g., Miyatake, 1980, 1992; Day, 1982a,b; Mikumo *et al.*, 1987; Harris and Day, 1993; Olsen *et al.*, 1997; Madariaga *et al.*, 1998). The method can be used to study rupture propagation in heterogeneous elastic media and is very efficient. An advantage of finite differences is that the operator $\Delta\boldsymbol{\Sigma}$ in Eq. (6) does not to have to be computed explicitly. In the FD method, all that is needed is a numerical procedure that computes the stress change $\Delta\mathbf{T}$ given the slip $\mathbf{D}$ distribution at earlier times.

Numerous different implementations of the FD method have been presented in the literature, and it is beyond the scope of this chapter to cover them all. In general, FD methods used to model earthquakes can be divided into two types. The first type derives from the direct discretization of the second-order PDE obtained by substituting Eq. (3) into Eq. (2). Methods of this kind were derived and greatly developed by Mikumo and Miyatake (1979), Miyatake (1980), Mikumo *et al.* (1987), and Mikumo and Miyatake (1993). The other approach, the staggered grid velocity–stress formulation, was developed by Madariaga (1976) to study dynamic rupture problems and is based on the discretization of the system of Eq. (4). The staggered grid method is characterized by low numerical dispersion and the fact that no derivatives of media parameters are needed. The latter is a strong advantage over FD implementations of the second-order displacement formulation of the wave equation where accuracy is lost in the computation of derivatives of media parameters near significant gradients in the model. Olsen *et al.* (1995a) and Olsen and Archuleta (1996) demonstrated the efficiency of the fourth-order formulation of the velocity–stress method by computing wave propagation around a kinematically defined rupture in a large-scale 3D model.

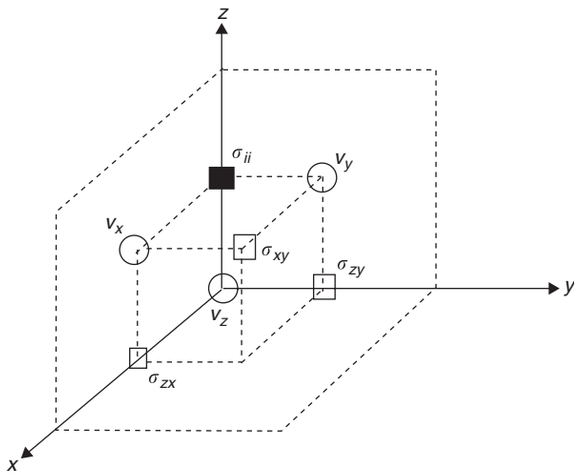

FIGURE 4 A cubic element of the 3D finite difference grid used in the dynamic modeling of a planar shear fault. σ and **v** depict the components of the stress tensor and particle velocity, respectively. (Reproduced with permission from Madariaga *et al*., 1998; fig. 9, p. 1192.)

The velocity–stress FD method is illustrated in Figure 4; stress and velocities are defined at alternating half-integer time steps. At time $t_N = N\,\Delta t$, particle velocity v is computed from previously calculated stress components. At the next half-time step $t_{N+1/2} = \left(N + \frac{1}{2}\right)\Delta t$, stress σ is updated using the velocity field computed at time t_N. Thus as time increases, velocities and stresses are computed at alternate times. Because stress and velocities are computed from Eq. (4) using centered fourth-order finite differences, the grid is also staggered spatially as shown in Figure 4. Madariaga *et al*. (1998) extended the FD method presented by Olsen (1994), Olsen *et al*. (1995a), and Olsen and Archuleta (1996) in order to study dynamic rupture propagation on a planar shear fault embedded in a heterogeneous half-space. We will use their "thick fault" boundary condition to illustrate important dynamic rupture phenomenology in this section, although alternate implementations exist. Current developments include the coupling of a BIE solution for slip and stress on the fault to a finite difference computation of radiated waves (Olsen *et al*., in preparation).

3. Phenomenology of Rupture Models with a Single Length Scale

We start the study of seismic ruptures from a very simple earthquake model that is a sort of classic test model inspired by Kostrov's (1964) study of a self-similar circular shear crack. We study the spontaneous propagation of a seismic rupture starting from a circular asperity that is ready to break. The asperity is surrounded by a fault surface uniformly loaded at a stress level that is less than the peak stress in the slip weakening friction law [Eq. (12)]. These are very similar conditions to those used by Day (1982b) and Das (1981) to start rupture. There are two main reasons to proceed this way: First, if the asperity is too small, rupture will start and stop immediately. For rupture to expand, stress must be high over a finite zone, sometimes called the minimum rupture patch. The other reason why rupture has to start from a finite-size asperity is that, if the stress field were uniform, rupture would occur instantaneously or grow at the maximum possible velocity from an arbitrary point on the fault. This is unrealistic and not supported by observations. Finally, it is assumed that fault rupture must occur at stress levels that are below the yield stress except for a small number of isolated asperities. In the following examples there is only one such asperity, even though rupture starting from several locations is possible (e.g., Day, 1982b; Olsen *et al*., 1997).

3.1 Dimensional Analysis

The following discussion uses nondimensional variables. This has the advantage of clearly showing how different variables scale with stresses and distances. We choose the following dimensional variables:

- Distances along the fault are measured in units of Δx, the grid interval.
- Wave velocities are measured in units of β, the shear wave velocity.
- Stress is measured in units of T_u, the peak frictional resistance (yield stress) in the friction laws described in Eqs. (12) and (13).

All other dimensions are determined by the previous three. In particular:

- Time is measured in units of $\Delta t = H\,\Delta x/\beta$, where β is the shear wave velocity. H is the so-called CFL (Courant–Friedrich–Lewy) parameter that controls stability of the numerical method. In our simulations it was usually taken as 0.25 in order to insure stability and sufficient accuracy.
- Displacement is measured in units of $T_u/\mu \times \Delta x$.
- Particle velocities are measured in units of $T_u/\mu \times \beta$.

Slip and slip rate are normalized by $2T_u/\mu \times \Delta x$ and $2T_u/\mu \times \beta$. The factor of 2 is not really necessary but follows a tradition in seismological publications. It is also assumed that the P-wave velocity α is equal to $\sqrt{3}\beta$. Finally, D_c, the slip weakening distance in Eq. (12) is measured in units of slip (i.e., $2T_u/\mu \times \Delta x$), and V_0, the rate weakening parameter, is measured in units of slip rate (i.e., $2T_u\mu \times \beta$). We have followed seismological tradition and used the grid length, Δx, to scale fault length, instead of a physical length such as the slip weakening distance D_c. The reason is that until recently most simulations

of 3D seismic ruptures used a grid-dependent fracture criterion introduced by Das and Aki (1977a) and attributed to Irwin.

3.2 A Circular Fault Model

In our first model we study rupture propagation where the initial stress distribution is symmetric about the origin. We force rupture to stop once it reaches a circular distance R. Rupture resistance, represented by T_u and D_c, is perfectly uniform. We initiate the rupture from a finite asperity of radius R_{asp}. Rupture velocity is not constant but is determined from the friction law. Our solutions are not self-similar and, as already illustrated by Das (1981), Day (1982b), Virieux and Madariaga (1982), and others, spontaneous ruptures do not maintain simple elliptical shapes as they grow.

The circular fault has a radius $R = 50 \times \Delta x$, starting from a concentric asperity of radius $R_{\text{asp}} = 6 \times \Delta x$, $D_c = 4$, and stress inside the asperity was $T_{\text{asp}} = 1.2 \times T_u$ and $T_{\text{ext}} = 0.8 \times T_u$ outside. Snapshots of the slip rate are shown in Figure 5 at several successive instants of time. Time is measured in units of $\Delta t = H\,\Delta x/\beta$, where $H = 0.25$ as discussed earlier. From time steps $t = 17.5$ to 35, rupture is taking place inside the asperity, and is propagating away from the asperity for $t > 52.5$. We observe that rupture becomes spontaneously elongated in the vertical direction, which is also the direction of the initial stress. Thus, as already remarked by Das (1981) and Day (1982b), rupture tends to grow faster in the in-plane direction, which is dominated by mode II.

At time $t = 87.5$, rupture in Figure 5 has reached the unbreakable border of the fault in the in-plane direction, and at time $t = 105$ the stopping phases generated by the upper and bottom edges of the fault are moving toward the center of the fault. The snapshots after $t = 122.5$ show stopping phases propagating inward from all directions. The slipping patch in darker shading is now elongated in the antiplane direction, which is due to slower healing. At time $t = 140$ the in-plane stopping phases (moving in the vertical direction) have already reached the center of the fault and crossed each other. In the

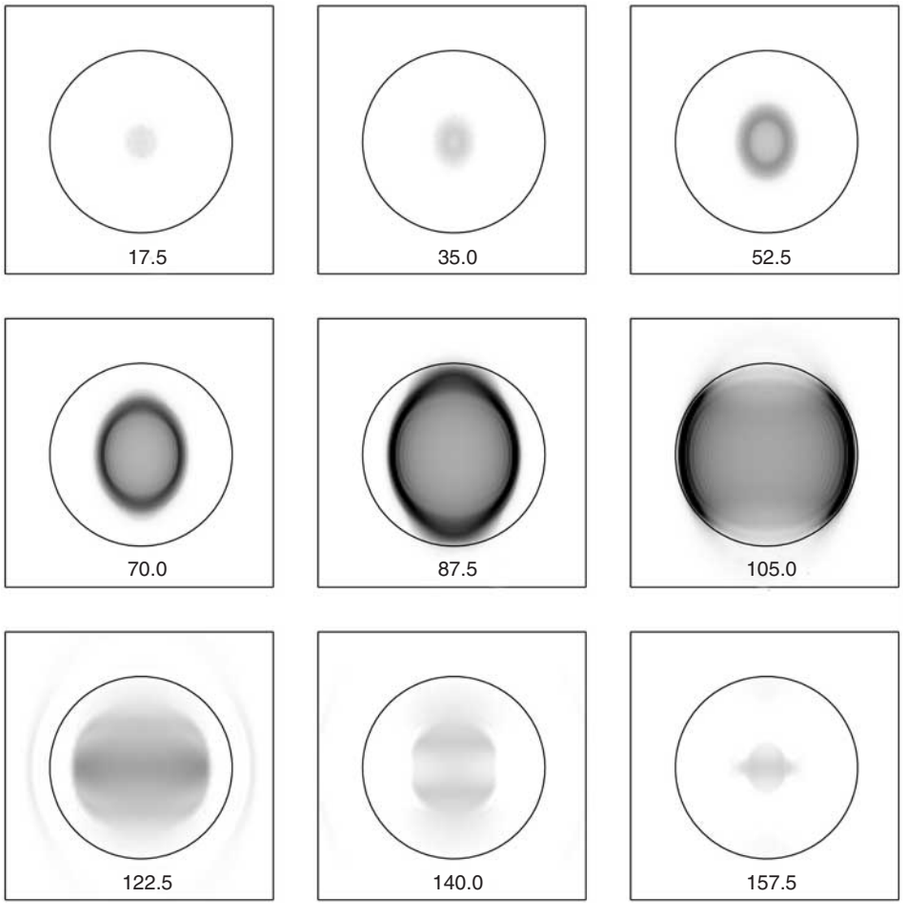

FIGURE 5 Snapshots of slip rate at successive instants of time for the spontaneous rupture of an overloaded asperity inside a circular fault (solid line). The nondimensional time for each snapshot is shown below each picture. (Reproduced with permission from Madariaga *et al*., 1998; fig. 9, p. 1192.)

last two snapshots, rupture continues in a small patch near the center of the fault that coincides with the initial asperity. However, slip rate has decreased to such small values that it is very likely contaminated with numerical noise.

3.3 Rectangular Fault

Now we turn to a model that starts in the same way as the circular fault from an overloaded asperity. However, here the unbreakable barrier forces rupture to expand in essentially one direction along a rectangular fault. We build this model as a prototype of rupture along a shallow strike-slip fault and use the same values for the friction laws as those for the circular crack simulation ($H = 0.2$; slip weakening distance $D_c = 4$; initial stress inside and outside the asperity $T_{\text{asp}} = 1.2 \times T_u$ and $T_{\text{ext}} = 0.8 \times T_u$, respectively; radius of the initial asperity $R_{\text{asp}} = 6 \times \Delta x$; for the rate-weakening simulations we used $V_0 = 0.03$ and $T_s = T_u$). Unfortunately, as pointed out by Heaton (1990) and discussed by Cochard and Madariaga (1996), there is no information about velocity weakening at high slip rates. The value chosen for V_0 is arbitrary and corresponds to rapid healing when slip rate becomes about 3% of the peak slip rate.

Color Plate 3 shows snapshots of the slip rate on the fault plane for simulations using slip weakening and slip weakening and rate weakening friction, respectively. The prestress on the fault is directed along the vertical (long) axis of the fault. In the simulation of part (a) with slip weakening but no rate weakening, we see the rupture emerging from the asperity with relatively slow healing (long "tail" trailing from the front). Rupture starts out slowly, accelerates toward the *S*-wave speed and, at a mature stage near time $t = 80$, suddenly "jumps" to the *P*-wave speed. The transition to supershear rupture speeds is an instability that develops from the in-plane direction and spreads laterally along the rupture front, producing a "bulge" observed in the snapshots after $t = 80$. Stopping phases emitted from the sides of the fault clearly control the duration of slip, as shown in snapshots at $t =$ 120 through 160. In the snapshot at $t = 160$, the stopping phases have reached the center of the fault just below the time label 160.

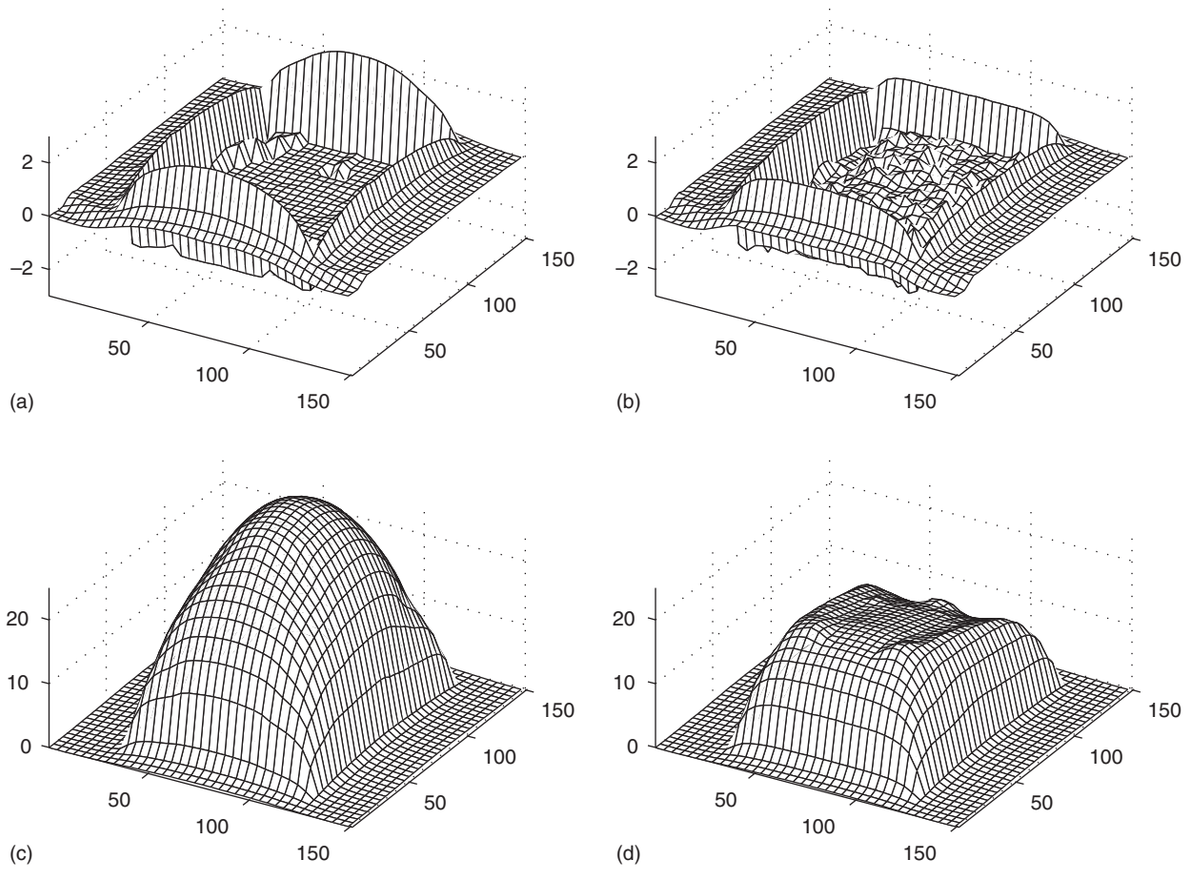

FIGURE 6 Final stress without (a) and with (b) rate weakening, and final slip without (c) and with (d) rate weakening, for the simulations shown in Color Plate 3(a) and (b). The plots clearly show a decrease in slip as well as the development of stress heterogeneity inside the fault due to rate weakening. (Reproduced with permission from Madariaga *et al.*, 1998; fig. 12, p. 1195.)

The situation is quite different with the use of a rate-dependent friction law, where the slip rate tends to concentrate in narrow patches (Part b). Compared to Part (a), the rupture front is narrower and clearly delineated. Well before the arrival of stopping phases from the sides of the fault, slip rate has become very small near the center of the asperity. Rupture takes the shape of a band. As time increases and rupture is controlled by the edges of the fault, the rupture front becomes narrow and localized. This is similar to the behavior predicted by Heaton (1990).

The other major difference introduced by rate-dependent friction is that, behind the rupture front, stress becomes heterogeneous. It appears that the rupture leaves a wake of complexity after its passage. This complexity is apparent in the distributions of both slip (Fig. 6c,d) and stress drop (Fig. 6a,b). The development of stress heterogeneity in the wake of the rupture front is an essential feature of rate weakening as proposed by Carlson and Langer (1989) for the BK model. It was shown by Cochard and Madariaga (1996) that stresses become complex because rate weakening promotes early healing of the fault. When the fault heals rapidly, all heterogeneities become frozen on the fault and cannot be eliminated until the fault slips again. This process of generating heterogeneity was the similar to what Bak *et al*. (1987) had in mind when they proposed that earthquakes were an example of self-organized criticality. Finally, note that the faster healing caused by rate weakening friction decreases the slip significantly.

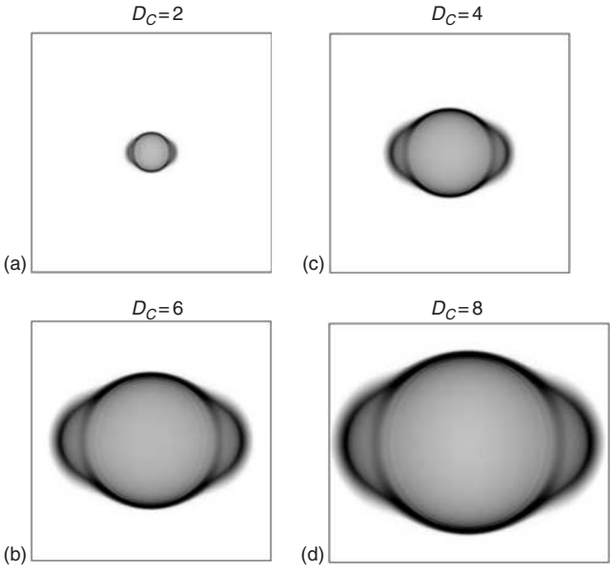

Au. Q: We've set this figure in single column. Pl. check if okay.

FIGURE 7 Scaling of rupture at constant load for spontaneous rupture starting from an overloaded asperity. The four snapshots show the distribution of slip rate on the fault at equivalent times for four different values of D_c. The initial asperity radius R as well as the instant of time of the snapshot all scale with D_c. (a) $D_c = 2$, $R = 3$, and $T = 140$; (b) $D_c = 4$, $R = 6$, and $T = 280$; (c) $D_c = 6$, $R = 9$, and $T = 420$; (d) $D_c = 8$, $R = 12$, and $T = 560$. (Reproduced with permission from Madariaga *et al*., 1998; fig. 6, p. 1186.)

3.4 Numerical Resolution and Scaling with the Slip Weakening Distance

An essential requirement for an accurate numerical method is that the numerical solution becomes independent of grid size beyond the use of a certain number of grid points per wavelength. The shortest physical distances are the radius of the asperity R and the width of the rupture front. The latter depends on the slip weakening distance D_c as shown by Ida (1972), Andrews (1976b), and Day (1982b). For 2D faults and for the slip weakening law (12) this width, L_c, is

$$L_c = \frac{4\mu}{3\pi} \frac{T_u}{T_{\text{ext}}^2} D_c \tag{17}$$

We have assumed that the residual friction at high slip rates in Eq. (12) ($T_f = 0$) is zero. This expression is valid for a constant stress level T_{ext} outside the asperity.

In order to describe the convergence of the numerical method as the grid size is refined, consider a simple circular asperity, keeping all the parameters constant except the grid size and D_c. Stress inside the asperity is $T_{\text{asp}} = 1.8 \times T_u$, $T_{\text{ext}} = 0.8 \times T_u$ and $H = 0.20$. Replacing T_{ext} in Eq. (17) gives $L_c = 1.36 \times D_c \Delta x$. Figure 7 shows snapshots of the slip rate as a function of position on the fault at equivalent instants of time. Since Δx is used as the scaling distance, both the radius of the asperity R as well as the time of the snapshot have to be increased for increasing values of D_c. The four parts of the figure show snapshots for (a) $t = 140$ ($D_c = 2$, $R = 3$), (b) $t = 280$ ($D_c = 4$, $R = 6$), (c) $t = 420$ ($D_c = 6$, $R = 9$), and (d) $t = 560$ ($D_c = 8$, $R = 12$). The external rectangles define the size of the grid, 256×256 for D_c from 2 to 6 and 300×256 for $D_c = 8$. Note the scaling of the figures—the snapshot for $D_c = 8$ is precisely twice as large as as that for $D_c = 4$. Clearly, the degree of resolution improves as D_c increases.

From a close examination of these snapshots and several others, we concluded that fourth-order finite difference simulations are contaminated by numerical noise when $D_c < 4\Delta x$, and that numerical simulations are stable and reproducible for $D_c > 6\Delta x$ ($L_c > 7\Delta x$). For 3D simulations, this is a rather large number that requires the use of very dense grids for accurate simulation of spontaneous rupture.

4. Earthquake Scaling Laws

In the previous section we illustrated spontaneous rupture starting from a circular asperity of radius R_{asp} that is ready to break (with stress T_u) and is surrounded by a fault surface. For convenience in numerical modeling, we scaled all physical

quantities by the grid interval Δx. Obviously this is not satisfactory in actual applications to earthquakes. The first earthquake scaling law was proposed by Aki (1967), who pointed out a relation between magnitudes at 1 Hz and at 20 sec, assuming that all earthquakes have a similar spectrum that depends on a single scaling variable, the size of the fault. This scaling law was later reformulated by Brune (1970) in the form of a universal shape for the spectrum of *S*-wave radiation.

The scaling laws can be derived by a simple dimensional analysis of the boundary value problem for an earthquake source in a uniform, infinite elastic medium. In such a simple medium there are only three independent physical dimensions: a length or geometric scale, a stress or dynamic scale, and the time scale. In elastodynamics the time scale is not independent of the length scale, since the two are connected by the speed of elastic waves. Adopting the shear wave speed β as the scale for velocities, and a measure of stress drop $\Delta\sigma$ as the stress scale, the only other free dimension is a length scale for the fault. The appropriate choice for the length scale is the overall size of the fault, its radius for a circular fault, or a characteristic dimension of stress distribution for complex sources. Once these variables are fixed, all other parameters can be scaled with respect to them. Thus, for instance, slip on the fault must scale like the characteristic length L times the ratio of the characteristic stress drop $\Delta\sigma$ to the elastic constant μ. Similarly, slip rate on the fault scales as the same ratio $\Delta\sigma/\mu$ times the wave speed β. All other physical quantities can be derived from these as shown in Table 1.

Studies of many earthquakes under completely different tectonic conditions, for shallow and deep sources, show that stress drop varies over at most two orders of magnitudes, while L varies over a wide range. As a consequence, seismic moment M_0 scales roughly with the cube of the fault size L for moments 10^{10}–10^{21} N m (moment magnitude $M_W = 8.0$). Beyond this magnitude there are serious uncertainties in the scaling law, but it is likely that very large earthquakes scale differently, in particular where ruptures are limited to a narrow zone near the surface of the Earth.

TABLE 1 Scaling of Different Physical Quantities from a Simple Fault Model as a Function of the Three Fundamental Parameters Length, Stress Drop, and Shear-wave Speed [a]

Variable	Symbol	Expression
Length	L	
Stress drop	$\Delta\sigma$	
Shear wave speed	β	
Slip	D	$\Delta\sigma/\mu \times L$
Slip rate	$\dot{D}$	$\Delta\sigma/\mu \times \beta$
Fault surface	S_0	L^2
Duration of radiation	T	L/β
S-wave corner frequency	f_c^S	β/L
P-wave corner frequency	f_c^P	α/L
Seismic energy	E_s	$\Delta\sigma^2/\mu \times L^3$
Seismic moment	M_0	$\Delta\sigma L^3$
Fracture energy	G	$\Delta\sigma D_c$

[a] Other groups of three fundamental units can be chosen, but this is the standard choice in seismology.

4.1 Other Length Scales

We have already seen in the discussion of numerical modeling that overall fault size is not the only length scale that is important in understanding earthquakes. The minimum slip patch—the minimum coherent zone of the fault that may rupture dynamically—is an important independent characteristic size of earthquake sources. Like all other length scales, this minimum patch size scales directly with the slip weakening distance D_c, the minimum slip necessary for friction to reduce to the kinetic friction on the fault. The exact nature of D_c is subject to debate, but the existence of such a length is absolutely necessary for the rupture problem to be physically well posed. Estimates of D_c and its associated minimum patch length scale $l = (\mu/\Delta\sigma)D_c$ vary widely, but it must be a small fraction of the overall length L. According to some authors, D_c is a property of the friction law to be determined from experiments on rock friction (see, e.g., Dieterich, 1978, 1979; Ruina, 1983); for others, D_c scales with the roughness of the fault surfaces, which in turn scales with earthquake size (Ohnaka and Kuwahara, 1990; Ohnaka and Shen, 1999). These two very opposite views emphasize different properties of earthquakes. For those authors who believe that D_c is a property of the fault zone, a universal friction law that describes the tribology of the fault must exist independently of the final size of the earthquake. This is consistent with most friction experiments carried out by the school of Dieterich, Ruina, and others.

For other authors, D_c is the result of rupture scaling over a broad range of magnitudes. Large earthquakes can occur only if D_c becomes large; otherwise they simply stop as first proposed by Aki (1979). Unfortunately it is not possible to settle this argument from seismic data alone because of the lack of high-quality near-field strong motion records. The current resolution of near-field observations is about 0.5 Hz, which translates into a shear wavelength of the order of 6–7 km and a slip weakening distance of $D_c \simeq 10^2$ cm (Ide and Takeo, 1997; Olsen *et al.*, 1997; Day *et al.*, 1998; Guatteri and Spudich, 1998b). This is too coarse to detect any scaling of D_c with earthquake size at the present time.

4.2 Scaling of Energy and Rupture Resistance

The previous discussion indicates that earthquake phenomena cannot be characterized by a single length scale unless, of course, the slip weakening distance scales with the size of the earthquake. Let us explore some of the consequences of small-size scaling for rupture dynamics through a simple fracture model.

Let us define rupture resistance, or energy release rate, which for the simple slip weakening friction model (12) is

given by

$$G = \frac{1}{2} T_u D_c \tag{18}$$

This is the amount of energy that is needed to produce a unit area of slipping fault. In most fracture studies this number is assumed to be a material property. However, Ohnaka and Shen (1999) present strong evidence that this may not necessarily be the case.

4.2.1 Rupture Initiation

A sensitivity analysis of the effect of changing rupture resistance on rupture propagation made by Madariaga and Olsen (2000) shows that there are two regimes that are controlled by a single nondimensional number:

$$\kappa = \frac{T_e^2}{\mu T_u} \frac{R_{\text{asp}}}{D_c} \tag{19}$$

where R_{asp} is the radius of the minimum asperity size (Madariaga and Olsen, 2000). This parameter can be derived from Andrews's (1976a) relation (17). As shown by Madariaga and Olsen (2000), using the calculations of Andrews (1976a), κ is a measure of the ratio of available strain energy ΔW to energy release rate G defined in Eq. (18). The strain energy change in a zone of radius R, uniformly loaded by an initial stress T_e is

$$\Delta W = \frac{1}{2} \langle D \rangle T_e \simeq \frac{T_e^2}{\mu R} \tag{20}$$

where $\langle D \rangle$ is the average slip on a fault of radius R and stress drop T_e. Thus $\kappa \simeq \Delta W/G$. An essential requirement for rupture to grow beyond the asperity is that $\kappa > \kappa_c$, where the critical value of κ for the circular asperity can be derived from the study by Madariaga and Olsen (2000), who computed numerically the critical radius R_c for fixed T_u, T_e, and D_c. They found that

$$\kappa_c = 0.60 \tag{21}$$

κ_c defines a bifurcation of the problem as a function of parameter κ. Another estimate of κ_c was obtained earlier by Day (1982a,b), who found $\kappa_c = 0.91$. The reason Day's estimate is larger than ours is that Day assumed that rupture could start only when energy balance around the whole perimeter of the asperity allowed rupture to start. As shown by Das and Kostrov (1983), however, rupture may start from the edge of the asperity and then surround the fault before breaking away from the asperity. For $\kappa < \kappa_c$, rupture does not grow beyond the initial asperity. For $\kappa > \kappa_c$, rupture grows indefinitely at increasing speed. This is a simple example of a pitchfork bifurcation.

There is a complication, however: as shown by Andrews (1976b), the rupture front makes a sudden jump to speeds larger than the shear wave speed if T_{ext} is larger than a certain fraction of the peak stress drop T_u. Transition to super-shear speeds is a complex bifurcation that needs much further study. Andrews (1976b) found that the jump to super-shear speed was due to the formation of a stress peak that runs at the shear wave speed ahead of the rupture front. This mechanism does not seem to operate for the transitions observed in 3D by Madariaga and Olsen (2000). In any case, super-shear ruptures in mode II (in-plane shear) are well documented by a number of experiments made by Rosakis *et al*. (1999). Madariaga and Olsen showed that the jump to super-shear speed occurs for a value of $\kappa > 1.3\kappa_c$; further discussion of this issue may be found in their paper. A final important remark is that the problem of rupture propagation from an initial asperity in a homogeneous medium under uniform stress has no other nondimensional control number than κ because this problem has exactly the five independent parameters that appear in the expression for κ. Andrews (1976b) used a different way of plotting the condition for rupture propagation and for super-shear speeds. It can easily be shown that his diagram can be reduced to a single nondimensional number κ.

4.2.2 Sustained Rupture Propagation

To characterize the conditions for sustained rupture propagation in a heterogeneous initial stress field, we consider a very simple rectangular asperity model. It consists of a homogeneous initial stress field that contains a long asperity of width W loaded with a longitudinal shear stress T_e. The asperity is surrounded by an infinite fault plane where stress is low, only $0.1\,T_u$, where as before T_u is the peak frictional stress. At time $t = 0$, rupture is initiated by forcing rupture over a circular patch of radius $R > R_c$, where R_c is computed from Eq. (19) using $\lambda_c = 0.42$. Depending on the values of T_e and the width W, rupture either grows along the asperity or stops very rapidly. We are again in the presence of bifurcation with a critical value. Similarly to Eq. (19), we define a nondimensional number

$$\kappa = \frac{T_e^2}{\mu T_u} \frac{W}{D_c} \tag{22}$$

where we have replaced the relevant length scale W in the denominator. We then verified numerically that ruptures stop for low values of $\kappa < \kappa_c$ and grow indefinitely for $\kappa > \kappa_c$, where κ_c is a numerically determined bifurcation point. As shown by Madariaga and Olsen (2000), $\kappa_c = 0.76$ for sustained rupture along a rectangular asperity. This value is slightly larger than $\kappa_c = 0.6$ for rupture initiation, a logical result explained by the fact that it is easier to propagate rupture on a uniformly loaded fault than on a fault loaded along a narrow asperity. Again, for a certain value of $\kappa > 1.3\kappa_c$, rupture grows initially at very high speeds and then jumps to a speed higher than the shear-wave velocity.

Color Plate 4, part (a) shows rupture propagation along the long rectangular asperity for three values of κ. Left and right panels show simultaneous snapshots of shear stress and slip. The top row shows snapshots for $\kappa < \kappa_c$. Rupture in this case

starts near the asperity and then stops immediately. D_c is large relative to the value of W. The second row shows stress and slip rate when κ is slightly supercritical. A rupture propagates along the asperity at sub-shear speeds. As the rupture propagates, the rupture zone extends slightly outside the asperity, leaving an elongated final fault shape. Finally, the bottom row shows snapshots when κ is about 1.2 times critical. Now the rupture front is running faster than the shear wave producing a wake that spreads somewhat into the lower prestress zone. Thus we are again in the presence of a bifurcation: It is not enough to initiate a rupture, the stress field has to be high enough to maintain the continued rupture propagation.

5. Dynamic Model of a Major Earthquake: The 1992 *M* 7.3 Landers, California, Event

The 28 June 1992, magnitude 7.3 Landers earthquake occurred in a remotely located area of the Mojave Desert in Southern California (Figure 8), but the rupture process has been extensively studied due to its large size, proximity to the southern California metropolitan areas, and wide coverage by seismic instruments. Several studies inverted the rupture history of this event from a combination of seismograms, geodetic and geologic data, and the overall kinematics of the seismic rupture are thought to be understood (Campillo and Archuleta, 1993; Abercrombie and Mori, 1994; Cohee and Beroza, 1994; Dreger, 1994; Wald and Heaton, 1994; Cotton and Campillo, 1995a), making the Landers earthquake an appropriate test case for dynamic modeling. The work described in this section is a summary of work by Olsen *et al*. (1997) and Peyrat *et al*. (2001).

5.1 Estimation of Initial Stress and Frictional Parameters

The fault that ruptured during the Landers earthquake can be divided into three segments: The Landers/Johnson Valley (LJV) segment to the southeast where the hypocenter was located; the Homestead Valley (HV) segment in the central part of the fault; and the Camp Rock/Emerson (CRE) segment to the northwest. For the numerical simulations, the three segments of the fault were replaced by a single 78 km long vertical fault plane extending from the surface down to 15 km depth. A free-surface boundary condition was imposed at the top of the grid.

The most important parameter required for dynamic modeling is the initial stress on the fault before rupture starts; all other observables of the seismic rupture, including the motion of the rupture front, are determined by the friction law. An

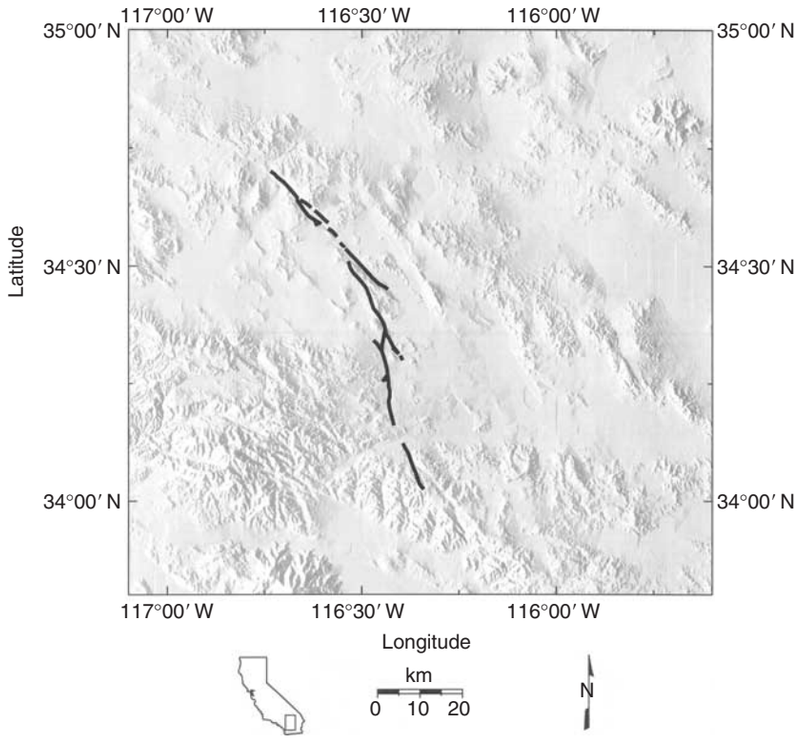

FIGURE 8 Topographic map showing the surface rupture from the 1992 Landers earthquake. The fault trace is depicted by the black lines.

initial stress field was estimated by Olsen *et al*. (1997) from the slip distribution inverted by Wald and Heaton (1994). They simply computed the stress drop from the slip distribution; the initial stress was the sum of a stress baseline of 5 MPa plus the stress drop reversed in sign. The method of computing the initial stress field is similar to that introduced by Mikumo and Miyatake (1995) and used by Beroza and Mikumo (1996) and Bouchon (1997) to study the stress field of several earthquakes in California.

The simple slip weakening friction law discussed in an earlier section was used in the dynamic simulations. Slip was assumed to occur only along the long dimension of the fault, and it was found that a constant yield stress level of 12 MPa and $D_c = 0.80$ m produced a total rupture time and final slip distribution in agreement with kinematic inversion results. Before the simulation the initial stress $\mathbf{T}^0$ on the fault was constrained to values just below the specified yield level (12 MPa) in order to prevent rupture starting from several locations. The same regional 1D model of velocities and densities as in Wald and Heaton (1994) was used in the numerical simulation. Rupture was forced to initiate by lowering the yield stress in a small patch of radius 1 km inside a high-stress region near the hypocenter toward the southern end of the LJV fault strand, as inferred from the kinematic results.

5.2 Rupture Propagation in a Heterogeneous Stress Field

Olsen *et al*. (1997) presented the first study on spontaneous rupture propagation in a realistic heterogeneous stress field on the Landers fault. They found that the rupture propagated along a complex path, predominantly breaking patches of high stress and almost completely avoiding areas of low or negative stress. The general rupture pulse resembles the fast, almost instantaneous self-healing phase with a finite slip duration proposed by Heaton (1990) for large earthquakes. However, the healing of the pulse was controlled by the local length scale of stress distribution, and not by slip rate weakening or fault width. Olsen *et al*. (1997) also succeeded in reproducing the main features of the low-frequency ground motion for amplitude and waveform at four strong-motion stations. These results suggested that considerable new information could be obtained about rupture dynamics through studies of spontaneous rupture propagation in estimates of the heterogeneous stress field for well-recorded large earthquakes.

5.3 Inversion of Strong Motion Data

In a recent dynamic inversion, Peyrat *et al*. (2001) used the stress field constructed by Olsen *et al*. (1997) to start the inversion of accelerograms for the initial stress field. Peyrat *et al*. used the strong motion data recorded in the vicinity of the Landers fault to invert for the details of the rupture process by trial and error. For every initial stress distribution they computed the spontaneous rupture process, starting from the same initial asperity at the southwestern end of the fault. During the iterations, the geometry of the fault and the slip weakening friction law did not change, so that $T_u = 12$ MPa and $D_c = 0.8$ m for all the models they tested.

The preferred initial stress from the Peyrat *et al*. (2001) study is shown in Color Plate 4(b), and Color Plate 3(c) compares the rupture propagation for the dynamic model to that for the kinematic model computed by Wald and Heaton. In the case of the dynamic model, soon after initiation rupture propagates slowly downward. After 7 sec it appears that the rupture almost dies but, soon after, it suddenly accelerates upward. It again slows down at 11 sec before jumping to a northern part of the fault and continuing onward. Finally, the rupture finished on the shallow northwest part of the fault after about 21 sec, in agreement with the kinematic inversion. The rupture shows a confined band of slip propagating unilaterally toward the northeast along the fault, as pointed out by Heaton (1990). The finite width of the fault promotes the formation of a pulse by confining the rupture laterally, preventing the development of a cracklike rupture. The main differences between the kinematic and dynamic models occur within the first 10 sec of propagation. The slip rate peak at 5–6 sec for the kinematic model appear later (at 9 sec) for the dynamic model. Nevertheless, the main part of the rupture history (13–17 sec) is very similar for both models. Part (c) of Color Plate 4 shows the final slip distribution on the fault. The dynamic rupture model reproduces a smooth version of the slip pattern used to compute the initial stress distribution.

Accelerograms at the recording stations were computed using a frequency–wavenumber summation method that is more economical than using finite differences to propagate waves from the source to the stations. Figure 9 shows a comparison of the synthetic seismograms generated by the best model of Peyrat *et al*. (2001). Both synthetic and observed seismograms are low-pass filtered to frequencies below 0.5 Hz. The main features of the low-frequency ground motion for amplitude and waveform are reproduced by the synthetic seismograms for the relatively stronger ground motion recorded in the forward rupture direction. The fits for the back-azimuth stations were not as good because the effects of propagation and fault geometry are enhanced at these stations.

The dynamic rupture model of the Landers earthquake is controlled by several friction parameters that are not measured but that may eventually be determined by inversion of seismic and geodetic data. For instance, the rupture speed and healing of the fault are critically determined by the level of the yield stress and the slip weakening distance. If the slip weakening distance is chosen less than about 0.6–0.8 m, the rupture duration and therefore rise times are much shorter than those obtained from kinematic inversion (Campillo and Archuleta, 1993; Abercrombie and Mori, 1994; Cohee and Beroza, 1994; Dreger, 1994; Wald and Heaton, 1994; Cotton and Campillo, 1995), while larger values produce a rupture resistance that prevents

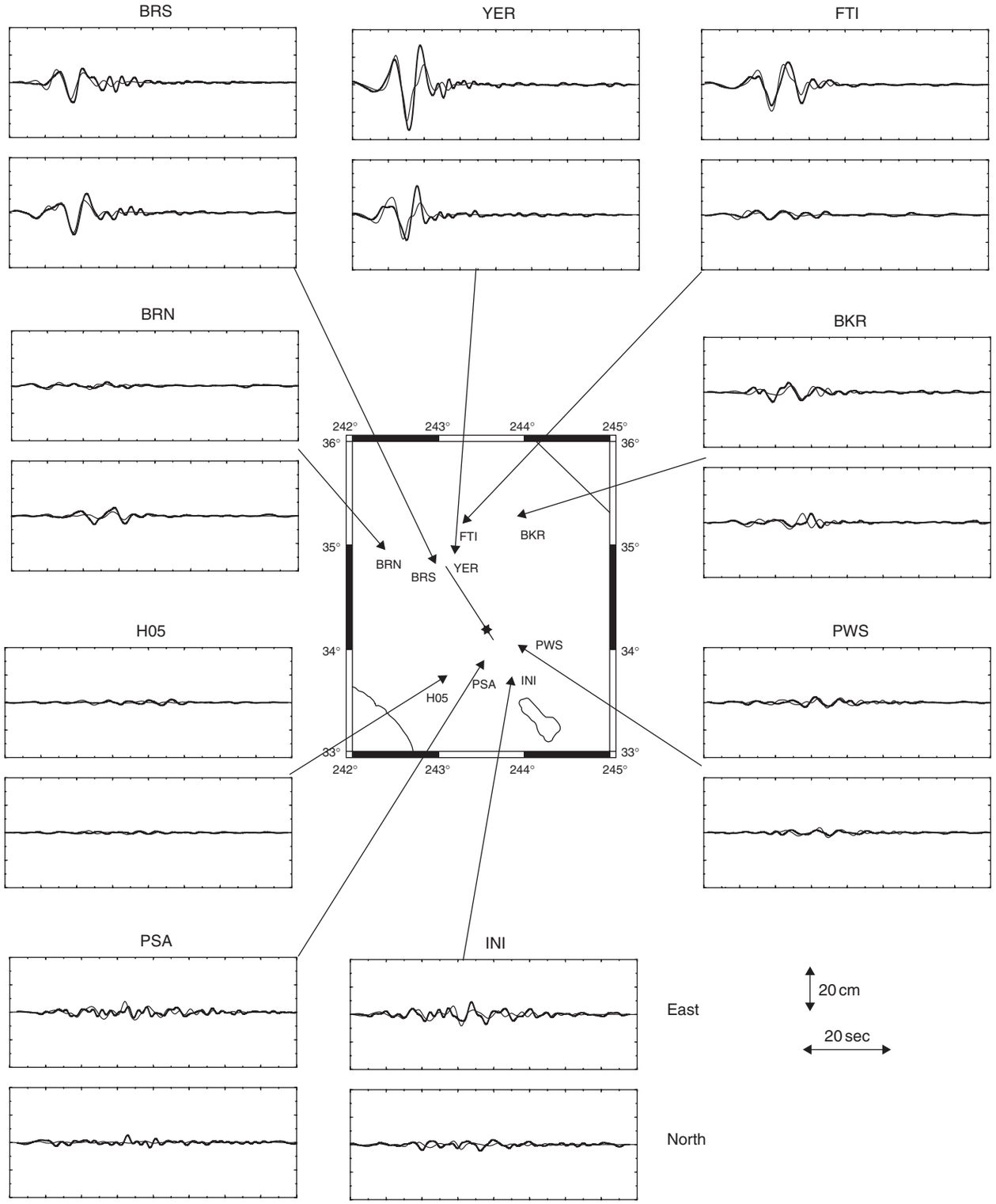

FIGURE 9 Comparison between observed ground displacements (thick traces) and those obtained for the preferred dynamic rupture model of the Landers 1992 earthquake (thin traces). For each station the upper trace is the east–west component of displacement and the bottom trace is north–south component. The time window is 80 sec, and the amplitude scale is the same for each station.

rupture from propagating at all. While the rupture duration and rise times are strongly related to the slip weakening distance, the final slip distribution remains practically unchanged for slip weakening distances that allow rupture propagation.

6. Earthquake Heterogeneity and Dynamic Radiation

Initial models of dynamic rupture propagation (e.g., Burridge and Knopoff, 1967; Andrews, 1976a,b) studied the frictional instability of a uniformly loaded fault. Very rapidly it was realized that heterogeneity was an essential ingredient of seismic ruptures and that the simple uniformly loaded faults could not explain many significant features of seismic radiation. Two models of heterogeneity were proposed in the late 1970s, the "asperity" model of Kanamori and Stewart (1978), based on a study of the Guatemalan earthquake of 1976, and the barrier model of Das and Aki (1977b) and Aki (1979). The differences between the two models were discussed in some detail by Madariaga (1979), who pointed out that it would be very difficult to distinguish between these two models from purely seismic observations. This remains true today. In the asperity model, it is assumed that the initial stress field is very heterogeneous because previous events have left the fault in a very complex state of stress. In the barrier model, heterogeneity is produced by rapid changes in rupture resistance so that an earthquake would leave certain patches of the fault (barriers) unbroken. It was quickly realized that barriers and asperities were necessary in order to maintain a certain degree of heterogeneity on the fault plane that could explain the properties of high-frequency seismic wave radiation, and to leave highly stressed patches that would be the sites of aftershocks and future earthquakes. Andrews (1980, 1981) went much further and suggested that this heterogeneity was absolutely necessary, otherwise earthquakes would become dominated by very low frequencies and could not produce observed accelerograms. Heterogeneity was studied in many ways by a number of authors during the early 1980s (e.g., Day, 1982b; Das, 1980; Kostrov and Das, 1989).

6.1 Generation of Cracks Versus Self-Healing Pulses

Heaton (1990) noticed that the instantaneous rupture area for large earthquakes is seldom larger than about 10% of the total fault area, so that seismic ruptures look more like a patch propagating across the fault compared to Kostrov's (1964) model of a self-similar shear crack. Heaton explained the pulselike behavior with a self-healing mechanism due to velocity weakening friction. Similar pulselike behavior has been reported from modeling a rectangular fault with a large aspect ratio due to stopping phases from the edges of the fault (Day, 1982a; Cotton and Campillo, 1995a). More recently, Beroza and Mikumo (1996), Ide and Takeo (1997), and Day *et al*. (1998) have shown that short rupture pulses may also be generated by the so-called geometrical constraint in which these short durations may simply reflect the stress heterogeneity on the fault. If stress is concentrated in small areas of the fault, the rupture process will reflect this heterogeneity and produce rupture pulses controlled by the size of these stress asperities.

Zheng and Rice (1998) characterized the conditions for generation of self-healing pulses in terms of the steady-state strength relative to the background stress in a velocity-weakening regime. They found that pulselike rupture occurs only for rather restrictive conditions of rate dependence. They furthermore suggested that the reason why most earthquakes fail to grow to a large size may be that the crustal stresses are too low on average to allow cracklike modes and continued rupture. In other words, most earthquakes fail to maintain rupture propagation because the driving stresses are too low and stop before producing a significant moment release.

6.2 Memory of Earthquake Rupture: Recurrent Events on a Fault

In this chapter we have concentrated our attention on the study of a single event without concern about earthquake recurrence or earthquake distributions. One of the main results obtained by Carlson and Langer (1989) is that for certain friction laws stress heterogeneity will be self-sustained, i.e., every event initiates in a complex state and leaves the fault loaded with a complex stress distribution. Cochard and Madariaga (1996) showed that this mechanism could also occur on two-dimensional shear faults but for a limited set of rate dependent friction laws. Only if healing were fast enough could heterogeneity develop spontaneously. The mechanism studied by Cochard and Madariaga (1996) produced heterogeneity but could not explain the Gutenberg–Richter distribution of events as a function of moment (or moment magnitude).

Nielsen *et al*. (2000) found that recurrent ruptures for a single planar fault with aspect ratio close to 1 and sufficiently low rupture resistance tended to produce a periodic cycle, always breaking the entire fault. However, if the dimension of the fault was increased with the same aspect ratio and friction, the regime became more complex and periodicity was lost. In the case of a long and narrow fault, i.e., $L/W > 10$, the pulse width $l_p \approx W$ was smaller than the maximum fault length L, and a degree of complexity was observed. Indeed, after a transient regime affected by the initial conditions, the fault settled into a recurrence pattern in which no rupture would reach the entire length of the fault, and a wide spectrum of event sizes was produced as opposed to the periodic cycle of fault-wide events observed for faults with aspect ratio close to 1. In other words, the recurrent earthquakes on the fault would generate an inherent complexity of the stress field that completely controlled the rupture conditions for the following events.

6.3 Signature of Friction in Radiated Waves

Is it possible directly to retrieve information about friction from strong motion data? To answer this important question we need to know how (or whether) the friction manifests a signature in the radiated wave field from earthquake rupture. Ide and Takeo (1997) estimated a depth-varying slip weakening distance of 1 m near the surface and 0.5 m at depth for the 1995 Kobe earthquake using inverse techniques. Olsen *et al*. (1997) found that a slip weakening distance of 0.8 m and a yield stress of 12 MPa generated rupture durations and seismograms in good agreement with kinematic inversion results and data, respectively, for the 1992 Landers earthquake. On the other hand, Guatteri and Spudich (1998b) concluded that there is a strong trade-off between peak stress and slip weakening distances. Actually, Peyrat *et al*. (2001) found that the energy release rate $G \simeq T_u D_c$, a product of the peak stress and the slip weakening distance, is all that can be retrieved from seismic data.

If indeed the signature of friction is detectable in strong-motion data, the retrieval of such information will be possible only when data are available in sufficient quality and quantity. In this case, an estimate of friction using inverse methods may be feasible. We expect that this will be an important topic of future research.

7. Conclusions

Thanks to improvements in speed and memory capacity of parallel computers it is no longer a problem to model the propagation of seismic ruptures along a fault, or a fault system, embedded in an elastic 3D medium. The enhanced computational power can be used to improve classical models in order to determine the grid size necessary to do reproducible and stable earthquake simulations. We show that the conditions are that the slip-weakening zone near the rupture front must be sampled by at least six grid points. This is clearly a limiting condition, but it is already possible to model earthquakes of magnitudes from 6 to 7.5 without unsurmountable problems.

Recent inversions of earthquake slip distributions using kinematic source models have found that very complex source distributions require an extensive reappraisal of classical source models that were mostly based on Kostrov's model of a self-similar circular crack. Ruptures in a fault with a very heterogeneous load follow very tortuous rupture paths. While on the mean the rupture propagates at a sub-shear speed from one end of the fault to the other, the rupture front may wander in any direction, following the areas of strong stress concentration and avoiding those areas with low stress or high rupture resistance. If this view of earthquake rupture is confirmed by future observations (we believe it will be) then many current arguments about earthquake complexity, narrow rupture pulses, earthquake distributions, etc., will be solved and we may concentrate on the interesting problem of determining which features of friction control stress complexity on the fault under all circumstances.

Acknowledgments

We thank Takeshi Mikumo and Joe Andrews for very detailed and helpful reviews. R. Madariaga's work was supported by CNRS (Centre National de la Recherche Scientifique) under contract 99PNRN13AS of the PNRN program. K.B. Olsen's work was supported by the Southern California Earthquake Center (SCEC). SCEC is funded by NSF Cooperative Agreement EAR-8920136 and USGS Cooperative Agreements 14-08-0001-A0899 and 1434-HQ-97AG01718.572726 through the NSF cooperative agreement EAR-8920136. This is ICS contribution 378-116EQ and SCEC contribution number 539.

References

Abercrombie, R. and J. Mori (1994). Local observations of the onset of a large earthquake: 28 June 1992 Landers, California. *Bull. Seismol. Soc. Am.* **84**, 725–734.

Aki, K. (1967). Scaling law of seismic spectrum. *J. Geophys. Res.* **72**, 1217–1231.

Aki, K. (1979). Characterization of barriers of an earthquake fault. *J. Geophys. Res.* **84**, 6140–6148.

Andrews, J. (1976a). Rupture propagation with finite stress in antiplane strain. *J. Geophys. Res.* **81**, 3575–3582.

Andrews, J. (1976b). Rupture velocity of plane strain shear cracks. *J. Geophys. Res.* **81**, 5679–5687.

Andrews, J. (1980). A stochastic fault model. I. Static case. *J. Geophys. Res.* **85**, 3867–3877.

Andrews, J. (1981). A stochastic fault model. II. Time-dependent case. *J. Geophys. Res.* **87**, 10821–10834.

Andrews, J. (1985). Dynamic plane-strain shear rupture with a slip-weakening friction law calculated by a boundary integral method. *Bull. Seismol. Soc. Am.* **75**, 1–21.

Aochi, H., E. Fukuyama, and M. Matsu'ura (2000). Spontaneous rupture propagation on a non-planar fault in 3D elastic medium. *Pageoph* **157**, 2003–2027.

Archuleta, R. and S.M. Day (1980). Dynamic rupture in a layered medium: the 1966 Parkfield earthquake. *Bull. Seismol. Soc. Am.* **80**, 671–689.

Bak, P., C. Tang, and K. Wiesenfeld (1987). Self-organized criticality. *Phys. Rev. A.* **38**, 364.

Bernard, P. and R. Madariaga (1984). A new asymptotic method for the modeling of near-field accelerograms. *Bull. Seismol. Soc. Am.* **74**, 539–557.

Beroza, G. and T. Mikumo (1996). Short slip duration in dynamic rupture in the presence of heterogeneous fault properties. *J. Geophys. Res.* **101**, 22449–22460.

Bouchon, M. (1997). The state of stress on some faults of the San Andreas system as inferred from near-field strong motion data. *J. Geophys. Res.* **102**, 11731–11744.

Bouchon, M. and D. Streiff (1997). Propagation of a shear crack on a nonplanar fault: a method of calculation. *Bull. Seismol. Soc. Am.* **87**, 61–66.

Burridge, R. and L. Knopoff (1967). Model and theoretical seismicity. *Bull. Seismol. Soc. Am.* **67**, 341–371.

Brune, J. (1970). Tectonic stress and the spectra of seismic shear waves from earthquakes. *J. Geophys. Res.* **75**, 4997–5009.

Campillo, M. and R. Archuleta (1993). A rupture model for the 28 June 1992 Landers, California, earthquake. *Geophys. Res. Lett.* **20**, 647–650.

Cao, T. and K. Aki (1984). Seismicity simulation with a mass-spring model and a displacement hardening-softening friction law. *Pageoph* **122**, 10–24.

Carlson, J. and J. Langer (1989). Mechanical model of an earthquake fault. *Phys. Rev. A* **40**, 6470–6484.

Cochard, A. and R. Madariaga (1996). Dynamic faulting under rate-dependent friction, *J. Geophys. Res.* **142**, 419–445.

Cohee, B. and G. Beroza (1994). Slip distribution of the 1992 Landers earthquake and its implications for earthquake source mechanics. *Bull. Seismol. Soc. Am.* **84**, 692–712.

Cotton, F. and M. Campillo (1995a). Frequency domain inversion of strong motions: application to the 1992 Landers earthquake. *J. Geophys. Res.* **100**, 3961–3975.

Cotton, F. and M. Campillo (1995b). Stability of rake: an evidence to partial stress-drop during the 1992 Landers earthquake? *Geophys. Res. Lett.* **22**, 1921–1924.

Cruse, M. (1988). "Boundary Element Method in Fracture Mechanics." Kluwer, Utrecht.

Das, S. (1980). A numerical method for the estimation of source time functions for general three-dimensional rupture propagation. *Geophys. J. Roy. Astron. Soc.* **62**, 591–604.

Das, S. (1981). Three-dimensional rupture propagation and implications for the earthquake source mechanism. *Geophys. J. Roy. Astron. Soc.* **67**, 375–393.

Das, S. and K. Aki (1977a). A numerical study of two-dimensional spontaneous rupture propagation. *Geophys. J. Roy. Astron. Soc.* **50**, 643–668.

Das, S. and K. Aki (1977b). Fault plane with barriers: a versatile earthquake model. *J. Geophys. Res.* **82**, 5658–5670.

Das, S. and D. Kostrov (1983). Breaking of a single asperity: rupture process and seismic radiation. *J. Geophys. Res.* **88**, 4277–4288.

Day, S.M. (1982a). Three-dimensional finite difference simulation of fault dynamics: rectangular faults with fixed rupture velocity. *Bull. Seismol. Soc. Am.* **72**, 795–727.

Day, S.M. (1982b). Three-dimensional simulation of spontaneous rupture: the effect of non-uniform prestress. *Bull. Seismol. Soc. Am.* **72**, 1881–1902.

Day, S.M., G. Yu, and D.J. Wald (1998). Dynamic stress changes during earthquake rupture. *Bull. Seismol. Soc. Am.* **88**, 512–522.

Dieterich, J. (1978). Time-dependent friction and the mechanics of stick-slip. *Pageoph* **116**, 790–806.

Dieterich, J. (1979). Modeling of rock friction. 1. Experimental results and constitutive equations. *J. Geophys. Res.* **84**, 2161–2168.

Dieterich, J. and B. Kilgore (1996). Implications of fault constitutive properties for earthquake prediction. *Proc. Natl. Acad. Sci. USA.* **93**, 3787–3794.

Dreger, D. (1994). Investigation of the rupture process of the 28 June 1992 Landers earthquake utilizing Terrascope. *Bull. Seismol. Soc. Am.* **84**, 713–724.

Fukuyama, E. and R. Madariaga (1995). Integral equation method for plane crack with arbitrary shape in 3D elastic medium. *Bull. Seismol. Soc. Am.* **85**, 614–628.

Fukuyama, E. and R. Madariaga (1998). Rupture dynamics of a planar fault in a 3D elastic medium: rate- and slip-weakening friction. *Bull. Seismol. Soc. Am.* **88**, 1–17.

Guatteri, M. and P. Spudich (1998a). Coseismic temporal changes of slip direction: the effect of absolute stress on dynamic rupture. *Bull. Seismol. Soc. Am.* **88**, 777–789.

Guatteri, M. and P. Spudich (1998b). What can strong motion data tell us about slip-weakening fault-friction laws? *Bull. Seismol. Soc. Am.* **90**, 98–116.

Geubelle, P. and J. Rice (1995). A spectral method for 3D elasto-dynamic fracture problems. *J. Mech. Phys. Solids* **43**, 1791–803.

Gu, Y. and T.-F. Wong (1991). *J. Geophys. Res.* **96**, 21677–21691.

Harris, R. and S. Day (1993). Dynamics of fault interaction: parallel strike-slip faults. *J. Geophys. Res.* **98**, 4461–4472.

Harris, R. and S. Day (1997). Effect of a low velocity zone on a dynamic rupture. *Bull. Seismol. Soc. Am.* **87**, 1267–1280.

Haskell, N.A. (1964). Total energy spectral density of elastic wave radiation from propagating faults. *Bull. Seismol. Soc. Am.* **54**, 1811–1841.

Heaton, T. (1990). Evidence for and implications of self-healing pulses of slip in earthquake rupture. *Phys. Earth. Planet. Inter.* **64**, 1–20.

Hirose, S. and J.D. Achenbach (1989). Time-domain boundary element analysis of elastic wave interaction with a crack. *Int. J. Num. Mech. Eng.* **28**, 629–644.

Ida, Y. (1972). Cohesive force across the tip of a longitudinal-shear crack and Griffith's specific surface energy. *J. Geophys. Res.* **77**, 3796–3805.

Ide, S. and M. Takeo (1997). Determination of the constitutive relation of fault slip based on wave analysis. *J. Geophys. Res.* **102**, 27379–27391.

Kanamori, H. and G.S. Stewart (1978). Seismological aspects of the Guatemala earthquake of February 4, 1976. *J. Geophys. Res.* **83**, 3427–3434.

Koller, M.G., M. Bonnet, and R. Madariaga (1992). Modeling of dynamical crack propagation using time-domain boundary integral equations. *Wave Motion* **16**, 339–366.

Kostrov, B. (1964). Self-similar problems of propagation of shear cracks, *J. Appl. Math. Mech.* **28**, 1077–1087.

Kostrov, B. (1966). Unsteady propagation of longitudinal shear cracks. *J. Appl. Math. Mech.* **30**, 1241–1248.

Kostrov, B. and S. Das (1989). "Principles of Earthquake Source Mechanics," Cambridge University Press.

Madariaga, R. (1976). Dynamics of an expanding circular fault. *Bull. Seismol. Soc. Am.* **66**, 639–667.

Madariaga, R. (1978). The dynamic field of Haskell's rectangular dislocation fault model, *Bull. Seismol. Soc. Am.* **68**, 869–887.

Madariaga, R. (1979). On the relation between seismic moment and stress drop in the presence of stress and strength heterogeneity. *J. Geophys. Res.* **84**, 2243–2250.

Madariaga, R. and K.B. Olsen (2000). Criticality of rupture dynamics in three dimensions. *Pageoph* **157**, 1981–2001.

Madariaga, R., K.B. Olsen, and R.J. Archuleta (1998). Modeling dynamic rupture in a 3D earthquake fault model. *Bull. Seismol. Soc. Am.* **88**, 1182–1197.

Mikumo, T. and T. Miyatake (1978). Dynamical rupture process on a three-dimensional fault with non-uniform friction and near-field seismic waves. *Geophys. J. Roy. Astron. Soc.* **54**, 417–438.

Mikumo, T. and T. Miyatake (1979). Earthquake sequences on a frictional fault model with non-uniform strength and relaxation times. *Geophys. J. Roy. Astron. Soc.* **59**, 497–522.

Mikumo, T. and T. Miyatake (1993). Dynamic rupture processes on a dipping fault, and estimates of stress drop and strength excess from the results of waveform inversion. *Geophys. J. Roy. Astron. Soc.* **112**, 481–496.

Mikumo, T. and T. Miyatake (1995). Heterogeneous distribution of dynamic stress drop and relative fault strength recovered from the results of waveform inversion. *Bull. Seismol. Soc. Am.* **85**, 178–193.

Mikumo, T., K. Hirahara, and T. Miyatake (1987). Dynamical fault rupture processes in heterogeneous media. *Tectonophysics* **144**, 19–36.

Miyatake, T. (1992). Reconstruction of dynamic rupture process of an earthquake with constraints of kinematic parameters. *Geophys. Res. Lett.* **19**, 349–352.

Miyatake, T. (1980). Numerical simulations of earthquake source process by a three-dimensional crack model. I. Rupture process. *J. Phys. Earth* **28**, 565–598.

Nielsen, S.B., J. Carlson, and K.B. Olsen (2000). The influence of friction and fault geometry on earthquake rupture. *J. Geophys. Res.* **105**, 6069–6088.

Okubo, P. (1989). Dynamic rupture modeling with laboratory-derived constitutive relations. *J. Geophys. Res.* **94**, 12321–12335.

Ohnaka, M. (1996). Non-uniformity of the constitutive law parameters for shear rupture and quasi-static nucleation to dynamic rupture: a physical model of earthquake generation processes. *Proc. Natl. Acad. Sci. USA* **93**, 3795–3802.

Ohnaka, M. and Y. Kuwahara (1990). Characteristic features of local breakdown near crack-tip in the transition zone from nucleation to dynamic rupture during stick-slip shear failure. *Tectonophysics* **175**, 197–220.

Ohnaka, M. and L.F. Shen (1999). Scaling of rupture process from nucleation to dynamic propagation: implications of geometric irregularity of the rupturing surfaces. *J. Geophys. Res.* **104**, 817–844.

Olsen, K.B. (1994). Simulation of three-dimensional wave propagation in the Salt Lake Basin. Ph.D. Thesis, University of Utah, Salt Lake City, UT.

Olsen, K., R. Archuleta, and J. Matarese (1995a). Three-dimensional simulation of a magnitude 7.75 earthquake on the San Andreas fault. *Science* **270**, 1628–1632.

Olsen, K.B., J.C. Pechmann, and G.T. Schuster (1995b). Simulation of 3-D elastic wave propagation in the Salt Lake Basin. *Bull. Seismol. Soc. Am.* **85**, 1688–1710.

Olsen, K.B. and R. Archuleta (1996). Three-dimensional simulation of earthquakes on the Los Angeles fault system. *Bull. Seismol. Soc. Am.* **86**, 575–596.

Olsen, K.B., R. Madariaga, and R. Archuleta (1997). Three dimensional dynamic simulation of the 1992 Landers earthquake. *Science* **278**, 834–838.

Peyrat, S., K.B. Olsen, and R. Madariaga (2001). Dynamic modeling of the 1992 Landers earthquake. *J. Geophys. Res.* **106**, 26467–26482.

Rice, J. and Y. Ben-Zion (1996). Slip complexity in earthquake fault models. *Proc. Natl. Acad. Sci. USA* **93**, 3811–3818.

Rice, J.R. and A.L. Ruina (1983). Stability of steady frictional slipping, *Trans. ASME, J. Appl. Mech.* **50**, 343–349.

Rosakis, A.J., O. Samudrala, and D. Coker (1999). Cracks faster than the shear wave speed. *Science* **284**, 1337–1340.

Ruina, A. (1983). Slip instability and state variable friction laws. *J. Geophys. Res.* **88**, 10 359–10 370.

Sato, H. and T. Hirasawa (1973). Body wave spectra from propagating shear cracks. *J. Physics Earth* **84**, 829–841.

Scholz, C. (1989) "The Mechanics of Earthquake and Faulting," Cambridge University Press.

Scholz, C. (2000). Evidence for a strong San Andreas fault, *Geology* **28**, 163–166.

Schmittbuhl, J., J.-P. Vilotte, and S. Roux (1996). A dissipation-based analysis of an earthquake fault model. *J. Geophys. Res.* **101**, 27741–27764.

Spudich, P. and L.N. Hartzell (1984). Use of ray theory to calculate high-frequency radiation from earthquake sources having spatially variable rupture velocity and stress drop. *Bull. Seismol. Soc. Am.* **74**, 2061–2082.

Spudich, P. (1992). On the inference of absolute stress levels from seismic radiation. *Tectonophysics* **211**, 99–106.

Spudich, P., M. Guatteri, K. Otsuki, and J. Minagawa (1998). Use of fault striations and dislocation models to infer tectonic shear stress during the 1995 Hogyo-ken Nambu (Kobe) earthquake. *Bull. Seismol. Soc. Am.* **88**, 413–427.

Townend, J. and M.D. Zoback (2000). How faulting keeps the crust strong. *Geology* **28**, 399–402.

Virieux, J. (1986). P-SV wave propagation in heterogeneous media: velocity-stress finite-difference method. *Geophysics* **51**, 889–901.

Virieux, J. and R. Madariaga (1982). Dynamic faulting studied by a finite difference method. *Bull. Seismol. Soc. Am.* **72**, 345–369.

Wald, D. and T. Heaton (1994). Spatial and temporal distribution of slip for the 1992 Landers, California earthquake. *Bull. Seismol. Soc. Am.* **84**, 668–691.

Wolfram, S. (Ed.) (1986). "Theory and Applications of Cellular Automata: Including Selected Papers, 1983–1986." World Scientific, Singapore.

Zheng, G. and J.R. Rice (1998). Conditions under which velocity-weakening friction allows a self-healing versus a crack-like mode of rupture. *Bull. Seismol. Soc. Am.* **88**, 1466–1483.